MAX-PLANCK-INSTITUT FÜR QUANTENOPTIK

Advanced Titanium Sapphire Laser
ATLAS

H. Baumhacker, A. Böswald, H. Haas, K.J. Witte, U. Andiel,
J. Bayerl, X. Dong, M. Dreher, K. Eidmann, M. Fischer, M. Hegelich,
M. Kaluza, S. Karsch, G. Keller, G. Pretzler, H. Stehbeck, G. Tsakiris

MPQ-Report
272

July 2002

Max-Planck-Institut für Quantenoptik
85740 Garching, Bundesrepublik Deutschland

MAX-PLANCK-INSTITUT FÜR QUANTENOPTIK

Advanced Titanium Sapphire Laser ATLAS

H. Baumhacker, A. Böswald, H. Haas, K.J. Witte, U. Andiel,
J. Bayerl, X. Dong, M. Dreher, K. Eidmann, M. Fischer, M. Hegelich,
M. Kaluza, S. Karsch, G. Keller, G. Pretzler, H. Stehbeck, G. Tsakiris

MPQ 272 July 2002

Abstract

The advanced Ti:sapphire laser system ATLAS is described in detail. It is based on a commercial version of Continuum and has been subsequently upgraded with respect to pulse energy, prepulse suppression, beam quality, and multi-wavelength use. Now, ATLAS represents a complex laser system with two different oscillators, the well-known Mira-oscillator and a two-colour oscillator, a regenerative amplifier, and two operating multipass amplifiers. A third multipass amplifier in ATLAS 50 is constructed. Using ATLAS 2 as a "front end", we also work on a new amplification scheme, called "Superradiant Amplification". The objective is to generate sub-10fs pulses of several ten mJ energy. In ATLAS 2, the available pulse energies are up to 300 mJ and in ATLAS 10 up to 800 mJ. In both ATLAS versions the pulse duration is 130 fs and the repetition rate amounts to 10 Hz. For ATLAS 50, we expect pulse energies of up to 4.5 J, but the shot rate is lowered to 1 shot per 10 minutes. The beam quality of ATLAS 2 is two times diffraction limited. When a f/3 off-axis parabolic mirror is used for focusing, a focal intensity of $4 \cdot 10^{18}$ W/cm^2 is achieved. To maintain the same beam quality in ATLAS 10, a novel adaptive optics scheme based on two deformable mirrors is integrated into the beam line. These compensate for the wave front aberrations picked up by the pulse in the final multipass amplifier. Using an identical f/3 off-axis parabolic mirror a fluence of $2 \cdot 10^{19}$ W/cm^2 has been achieved.

Contents

1. Introduction

The advanced titanium:sapphire laser facility (ATLAS) has been developed for the investigation of high-field interaction and atomic physics. It is a complex laser system based upon a commercial chirped pulse amplification (CPA) version processed by Continuum [1] in 1995 and well documented in [2].

The amplifying medium is titanium:sapphire (Ti:S), which is – due to a large bandwidth, a favourable saturation energy density, a high damage threshold and a good thermal conductivity – well suited to deliver fs-pulses in the multi-Terawatt range at high repetition rates.

During the years this commercial version was incessantly reworked in order to improve the output with respect to pulse energy, prepulse and ASE-suppression, beam profile and in concern with it the focusability of the laser beam. A lot of components were changed or added, e.g. a second, two-colour oscillator and a further multipass amplifier including beam imaging, and deformable mirrors.

The now existing laser system is composed of the following main components: two oscillators, a conventional and a two-colour one, a stretcher, a regenerative amplifier, multipass amplifier 1 and compressor 1, thus forming ATLAS 2 (see Fig. 12 and 12a) and in addition a second multipass amplifier and compressor which we call ATLAS 10 (see Fig. 19). Here two deformable mirrors are installed to homogenize the beam profile and to care for an optimised focusability because of growth and pump induced defects of the Ti:S crystal.

In conjunction with ATLAS 2, a brand-new amplifier type, the so-called superradiant amplifier [3,4], is investigated.

Whereas both ATLAS 2 and 10 are running at 10 Hz, the single-shot amplifier ATLAS 50 is constructed - but not yet in operation - which follows ATLAS 10 and multiplies the pulse energy by a factor of up to 5.

The complex ATLAS laser system is schematically depicted in Figure 1. The individual components will be described in detail in the following chapters.

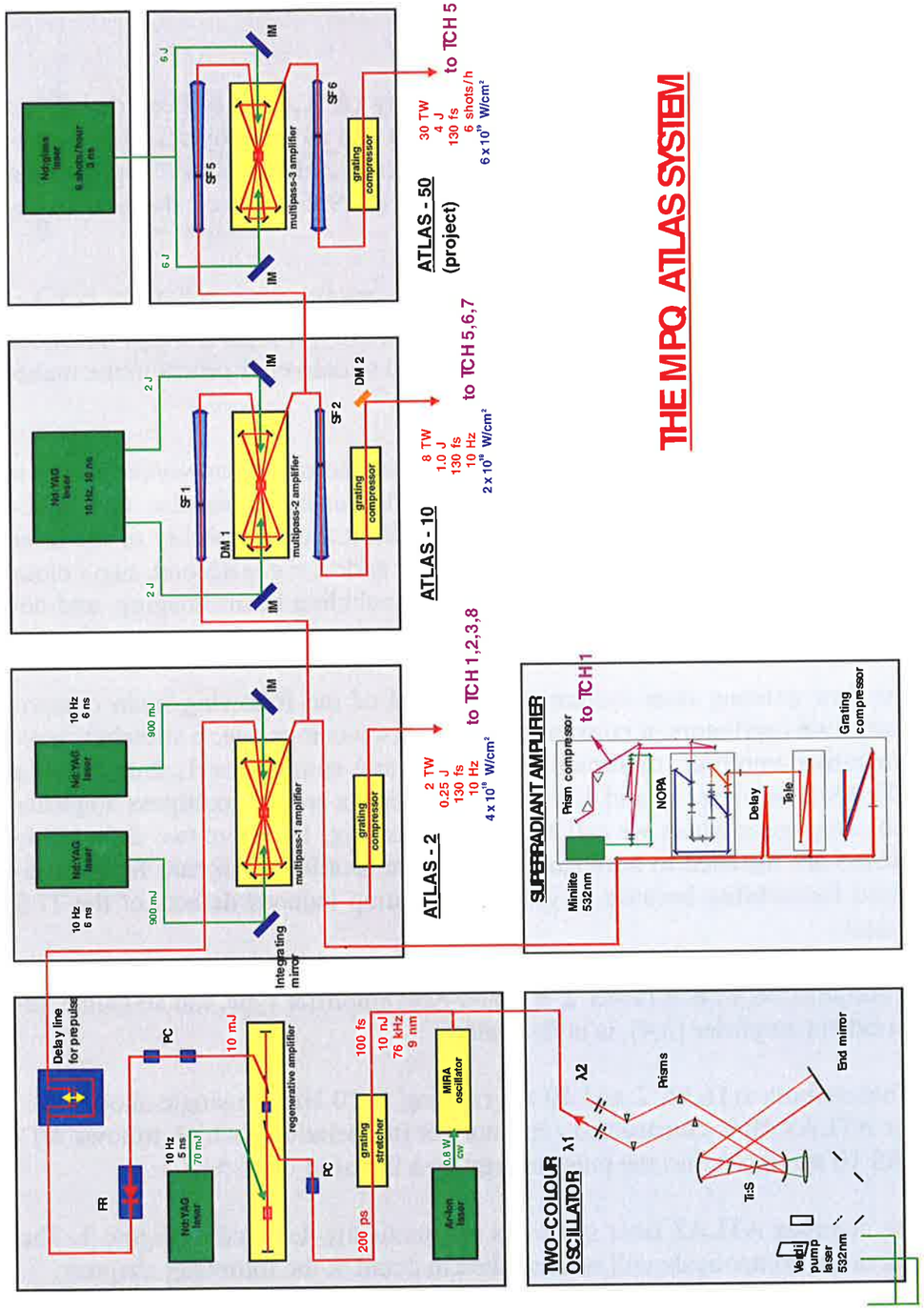

Fig.1: ATLAS laser system

2. The front end

2.1 The CPA system

On the one hand, the amplification of short, fs-pulses to high energy levels requires a gain medium with a broad enough bandwidth to accommodate the laser pulse spectrum and a superior energy storage, but on the other hand the laser intensity should be kept low enough to avoid nonlinear wavefront distortion. A measure of the nonlinear phase shift can be expressed by the factor

$$B = \frac{2\pi}{\lambda} \int_0^L n_2 I(z) dz ,$$

with n_2 being the nonlinear index of refraction. For maintaining the beam quality, it is essential to keep B to a minimum. Whereas for ns-pulses the B-value should not exceed 3 – 4, corresponding to a wavefront distortion of λ/2, the beam quality requirements for fs-pulses are even more stringent. The Marechal [5] expression defines the peak of the intensity I_p at the diffraction focus for small aberrations produced by nonlinear effects to be

$$I_p \propto 1 - B^2$$

That means that even for B < 1, e.g. B = 0.7 the intensity at the focus will be reduced by a factor of 2.

Materials with good energy storage, like Ti:S, need an input fluence of about 1 J/cm^2 for efficient energy extraction, which corresponds to an intensity level of I ≈ 10 TW/cm^2 for a 100 fs pulse duration. With that, B becomes extremely high, 100, which is by far above the acceptable level to attain homogeneous beam quality.

The stored energy, however, can be extracted at a moderate intensity level by applying the chirped pulse amplification technique [6]. Here a short pulse is created, that will be first stretched, then amplified, and finally recompressed to a short pulse with nearly the original duration (see Fig. 2). Herewith, by stretching the pulse, the input fluence is kept constant while reducing the intensity.

In ATLAS, a short pulse is generated with a duration of 100 fs and 10 nJ energy, which first is stretched by a factor of ≈1500 to a pulse duration of 150 ps, then amplified by about 8 orders of magnitude up to 0.4 J or 1.3 J, respectively, and finally recompressed to a nearly transform-limited pulse of 130 fs width.

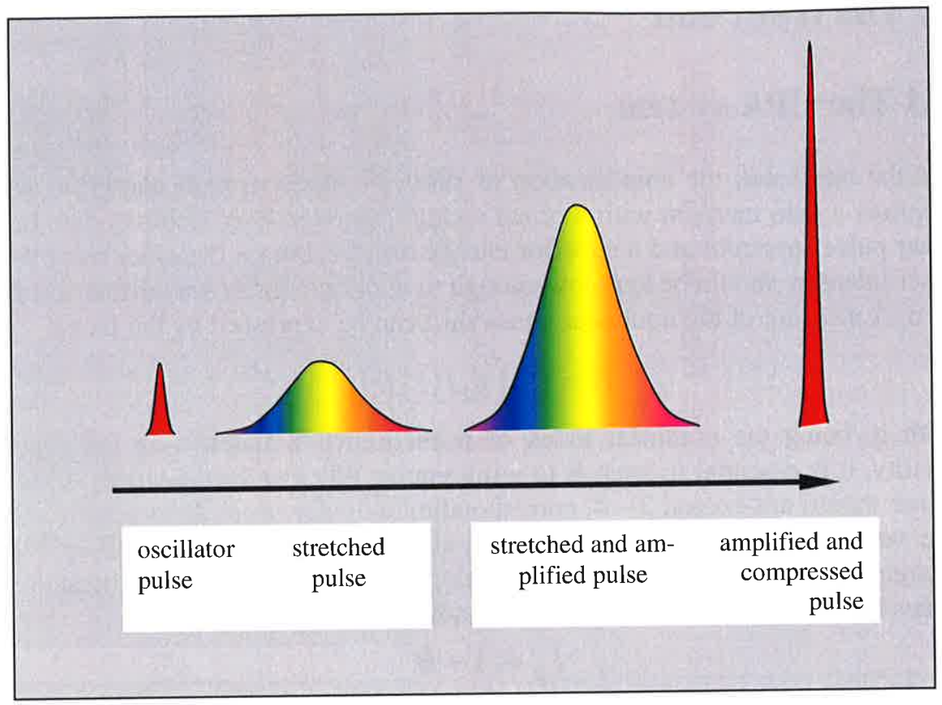

Fig. 2: CPA scheme

2.2 The generation of short pulses in a conventional oscillator

ATLAS normally starts with the Kerr-lens-modelocked Ti:S oscillator Mira [7] from Coherent (see Fig. 3). It is pumped by 8 - 10 W from a cw argon-ion laser and produces pulses with 10 nJ energy and 100 fs duration at a 76 MHz repetition rate. With an intracavity birefringent filter, it can be tuned over the wavelength range of 700 – 800 nm and for our purposes it is centered at 790 nm with a bandwidth of 10 nm. The time-bandwidth product is with $\nu\ \tau =$ 0.47 slightly larger than the time-bandwidth product of 0.32 for a $sech^2$ pulse, indicating the presence of some residual chirp. The contrast ratio – that is the ratio of the pulse peak intensity and that in the pulse wings – was measured to be at least 10^6 for more than 10 ps before and after the pulse maximum (see Fig. 4a and b) using the second-order autocorrelator shown in Fig. 5 and described in detail in [8]. The pulse contrast is limited by the dynamic range of

the autocorrelator, that is 10^6, and therefore is expected to be better; the theoretical limit is 10^{10}. The appertaining pulse spectra can be seen from Fig. 16.

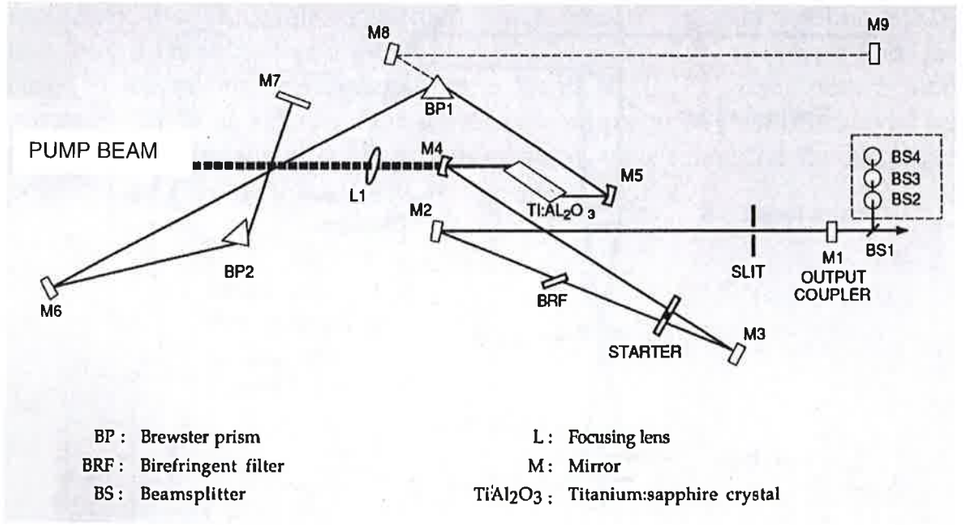

Fig. 3: Optical scheme of the Mira oscillator

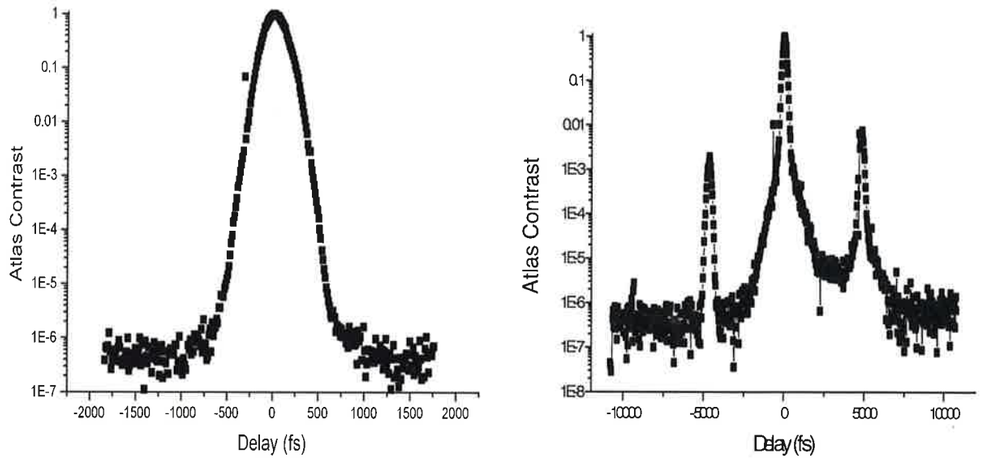

a) Short time scale

b) Time scale ±10 ps, (spikes in the wings are measurement artefacts)

Fig. 4: Characterisation of the Mira pulses

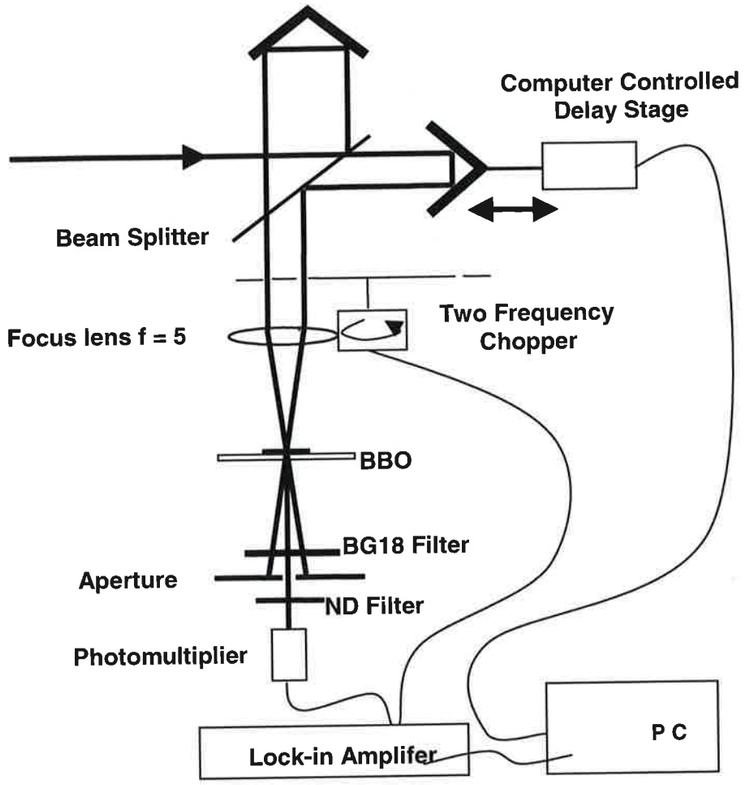

Fig. 5: Setup for high-dynamic range second-order autocorrelation measurements of fs-laser pulses

2.3 Two-colour oscillator

Many applications, e.g. the superradiant amplifier, require two laser pulses synchronized in time to better than a few femtoseconds with different wavelengths, pulse durations, and pulse energies.

Based on the work of Leitensdorfer et al. [9], a two-colour mode-locked Ti:S laser was developed which is integrated in the ATLAS system. Here two perfectly synchronized pulse trains independently operating at tunable wavelengths and pulse durations are produced in a single laser system. The combined effects of cross-phase modulation and negative group velocity dispersion are responsible for the strong pulse correlation in the synchronized regime [10].

As can be seen from Fig. 6, the laser consists of two asymmetric X-folded cavities, both sharing the gain medium, the high reflecting end mirror, and the folding mirrors. The prism compressors and output couplers can be adjusted separately, providing full wavelength independence. The gain medium is a 6-mm long 0.15 wt.%-doped Ti:S rod, which is pumped by two separated, focused pump beams originating from a Verdi V-10 [11] laser with a total power of 8.5 W at 532 nm. Fine tuning of both pump powers is achieved by rotation of the polarization of the pump beams, which modifies the absorbed power in the Ti:S medium.

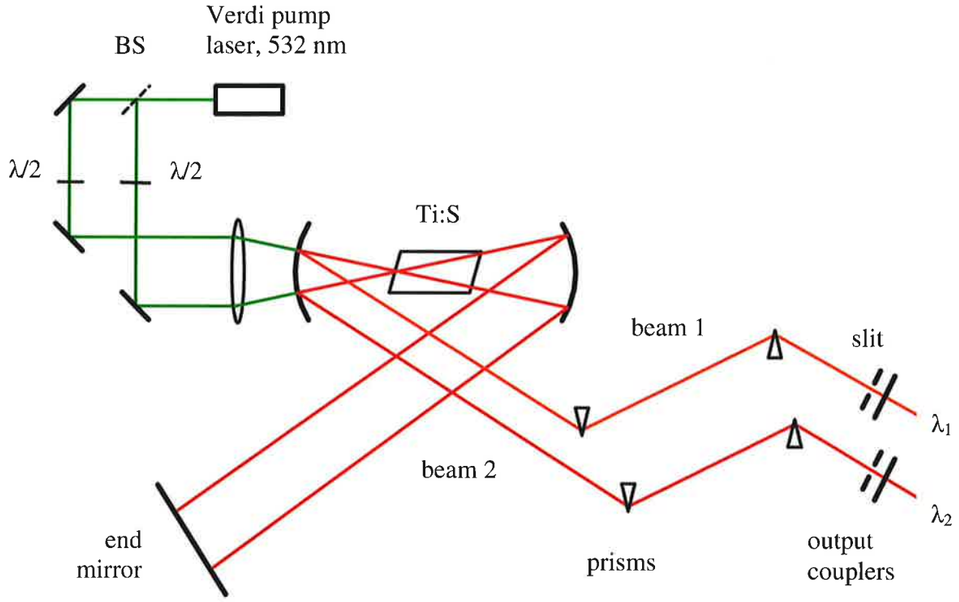

Fig. 6: Two-colour oscillator

Both resonators are formed by the common end and folding mirrors and, in addition, by separate dispersing fused-silica prism pairs, adjustable slits, and output couplers. The distance of the prisms are chosen such to generate pulse durations of ~35 fs in branch 1 and of ~100 fs in branch 2. Wavelength tuning – within the reflectivity range of both output mirrors – is achieved by adjustment of the second prisms and the two slits. Whereas in principle the wavelengths of both branches can be varied independently in the 50-nm range, for our purposes we fixed the center wavelength of beam 2 at 790 nm

and keep that of beam 1 tunable in-between 810 to 850 nm [12]. Fig. 7 shows some essential data obtained by tuning the wavelength of the short pulses in beam 1.

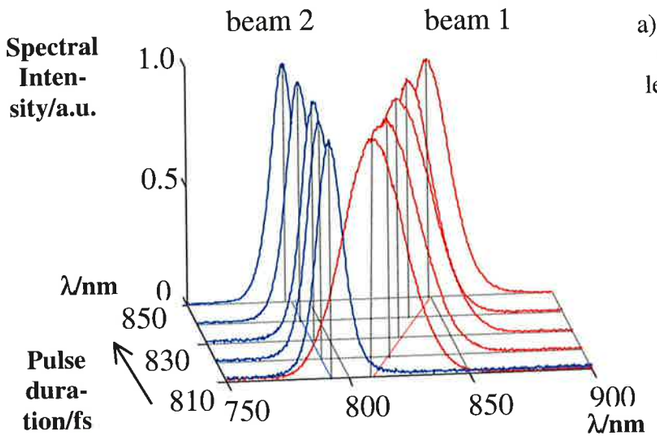

a) Spectra versus wavelength tuning

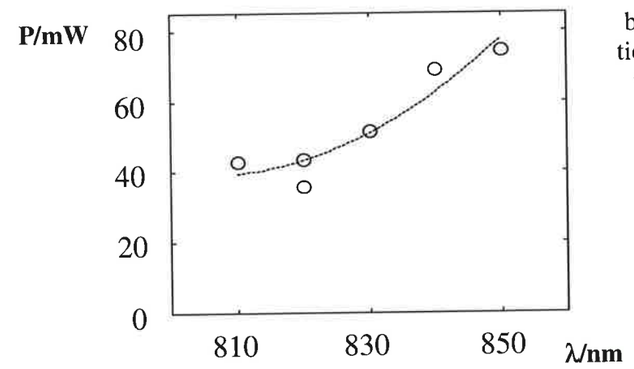

b) Pulse duration at different wavelengths

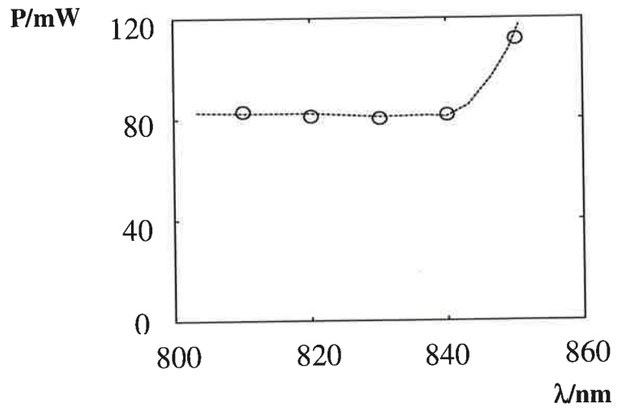

c) Output power at different wavelengths

Fig. 7: Measurements of the two-colour oscillator

The two pulse trains are synchronized when the round-trip times are equal. This is accomplished by varying the cavity length of branch 1. For that purpose, the position of the output mirror is changed until synchronisation is observed within an interval of 1 μm. The difference of the pulse repetition frequencies of $\nu_{1,2}$ = 76 MHz in the two branches can be made less than 2 Hz. We found that after a warm-up time of 1 hour and the two cavity lengths properly matched, the laser remains synchronized for several hours, supposed the temperature changes in the environment remains below 2.5 degrees.

The maximum achieved power is P = 120 mW in each branch, corresponding to a pulse energy of 1.6 nJ. This is - for the 790 nm beam - a factor of 6 less than the pulse energy in the conventional oscillator and must be taken into account in the amplifier construction. The single pulses have a good contrast ratio and show a pedestal power which was measured to be at least 5 orders of magnitude less than the peak power; the limitation is due to the dynamic range of the used second-order autocorrelator, which was 10^5 only.

2.4 Beam pointing stabilization

The beam directions both of the Mira oscillator and the two-colour oscillator deviate with time and temperature changes in the laboratory. This leads to changes of the seed overlap, i.e. the beam quality and instabilities in the regenerative amplifier, thereby deteriorating the beam quality. With a beam pointing stabilization system consisting of two quadrant detectors in combination with piezo-driven mirrors and implemented behind the Mira oscillator (see Fig. 8), the beam pointing drift could be lowered such, that the former necessary daily readjustment of the oscillator beam can be prolongated to once a month.

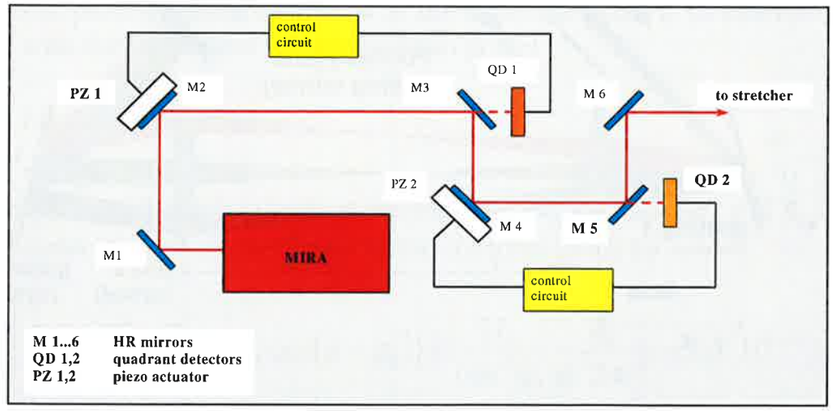

Fig. 8: Oscillator beam stabilization

2.5 Stretcher

A variety of simple and sophisticated stretcher configurations [13-16] are known. In ATLAS, a simple four-pass grating stretcher [13] is used to introduce a positive dispersion and hence to reliably stretch the seed pulse by a factor of about 1500 to 150 ps (see Fig. 9).

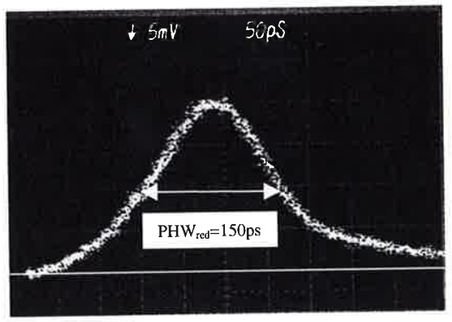

Fig. 9: TiS laser pulse shape measured at the exit of the stretcher using the fast photo diode Antel AR-S2 and the 1-GHz oscilloscope Tektronix 7104 with sampling plug-ins 7S11, 7T11A.

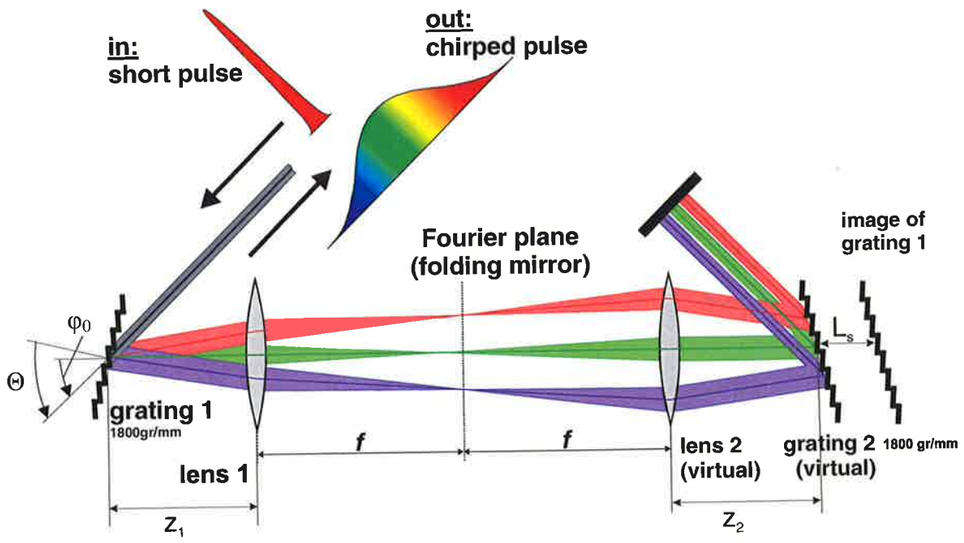

Fig. 10: Four-pass stretcher scheme

Fig. 10 shows the unfolded four-pass stretcher. In praxis, however, this stretcher system can be simplified by using only the left half of the components (Fig. 11) and in addition one folding mirror (HR-mirror 1) which is placed in the Fourier plane and reflects the beam back to a small rectangular mirror (HR-mirror 2) at the entrance. Consequently the four-pass stretcher consists of one single 1800-grooves/mm holographic grating, one 600-mm focal-length achromatic lens made of BK7 and SF5 glass, respectively, and two high-reflecting mirrors with a dielectric coating. The incident and diffracted angles for the grating are Θ=55° and φ_0=37.1°, respectively. The overall throughput efficiency could be raised from about 50 % to 72 % by replacing the original gold mirrors by dielectric coated ones and the original grating having a reflectivity of only 85 % by one with an enhanced reflectivity of 92 % [20].

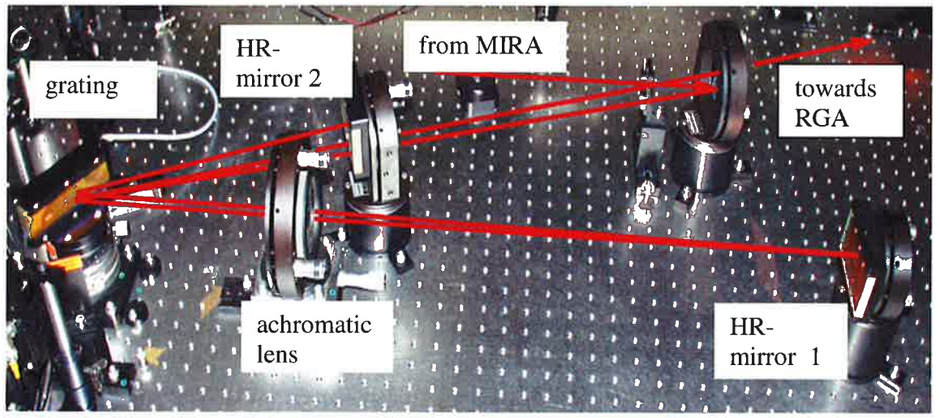

Fig. 11: Four-pass stretcher in ATLAS 2

The measured pulse duration of 150 ps of the stretched pulse is in satisfying agreement with the theoretical value (Gaussian pulse)

$$\tau_{Str} \cong 4\phi_0'' / \tau_{in} = 135\,ps\,,$$

where τ_{in} = 100 fs is the pulse duration prior to entering the stretcher and ϕ_0'' is the second-order dispersion coefficient of the stretcher given by

$$\phi_0'' = \left.\frac{d^2\phi}{d\omega^2}\right|_{\omega_0} = 2\frac{d}{d\omega^2}\{4f - L_S\cos(\varphi - \varphi_0)\} = \frac{2L_S}{\cos^2\varphi_0}\frac{\lambda_0^3}{d^2 2\pi c^2} = 3.4\cdot 10^{-24}\,fs^2$$

with $L_S = 2f - (z_1 + z_2) = 2 \cdot 0.6 - 0.54 = 0.66m$ (effective grating separation), $\lambda_0 = \frac{2\pi c}{\omega_0} = 0.79 \cdot 10^{-6} m$ (center wavelength), $\Theta = 55°$ (incidence angle), $d^{-1} = 1.8 \cdot 10^6 / m$ (inverse groove distance), and $\varphi_0 = \arcsin\left\{\frac{\lambda_0}{d} - \sin\Theta\right\} = 37.1°$ (diffraction angle).

3. Pulse amplification

After stretching, the laser pulses have to be amplified by at least 8 orders of magnitude to achieve output energies in the 1-J region. This can be performed by three different concepts. In the first, a regenerative amplifier (RA) is followed by one or more multi-pass amplifiers (MA), whilst in the second concept, MA's are used only. The third concept is totally different from both and it is based on the superradiant amplification (SRA) [4]. The SRA is under investigation in our group since two years, but it will last a while until it can be operated routinely in the ATLAS system. The RA and the MA's are widely used components and in the following there should be considered some pros and cons for both types.

The RA is in principle a TEM_{00} cavity around an amplifying medium, and the seed and amplified pulses are switched in and out by rotating the polarization of the laser beam. The essential argument in favour of the RA is that it provides an excellent beam quality, usually TEM_{00}. As to efficiency and pedestal formation, the RA is inferior to the MA. The poorer efficiency of the RA results from the presence of the losses in the Pockels cell and two not fully perfect polarizing beam splitters in the cavity. The many reflections occurring when the pulse is circulating in the cavity give rise to ghost pulses which are difficult to eliminate even with a series of Pockels cells following the RA. A further disadvantage is the higher level of the amplified spontaneous emission (ASE). Because of that the pulse leaving the cavity has hence a pretty strong pedestal.

In the MA there is used an angular multiplexing of the beam and because of space limitation the amount of transits is restricted. The usual argument brought up against the MA is the sensitivity of the output pulse energy versus fluctuations of the input pulse energy. However, this sensitivity can be made sufficiently small when in the last two passes through the crystal the fluence is close to or beyond the saturation energy density.

Inspite of the drawbacks, in ATLAS we use the RA - because it was built in

the commercial version we started from and an exchange did not appear feasible for reasons of time and costs – to enhance the pulse energy from the low level of about 1 nJ to the 10 mJ region and in addition two consecutive MA bring up the pulse energy to 350 mJ in the ATLAS 2 and 1.3 J in ATLAS 10, respectively. Whilst both versions are running at 10 Hz repetition rate, the also constructed but not in-operation version ATLAS 50 can fire only every 10 minutes.

4. ATLAS 2: Pulse amplification and compression

4.1 Regenerative amplifier

After the 76-MHz pulse train has passed the stretcher and the first Faraday isolator, a single pulse is switched into the RA cavity in a 10-Hz repetition rate with the aid of two Pockels cells, PC 1 just before the RA and the intracavity PC 2 (see Fig. 12 and 12a). The resonator is 1.7 m long and is formed by two highly reflecting, dielectric mirrors having radii of 10 m concave and 20 m convex, respectively. The radius of the thus formed beam waist is 2.2 mm. The Brewster-cut Ti:S crystal is 15 mm long with a 0.15 wt.% doping and is end-pumped with up to 100-mJ, 5-ns pulses of a frequency-doubled Continuum Surelite 1 laser. A 1:2.5 - telescope is used to match the pump-beam diameter to the beam waist and to image relay the pump beam from the exit of the pump laser into the Ti:S crystal, thus the pump fluence in the Ti:S crystal is about 1.5 J/cm^2. AR-coating of the Pockels cells and the coating of the 72°-polarizers are broadband. The Pockels cells are driven by half-wave voltage pulses of 6 kV / 5 ns from a thyratron pulser. The switched-in pulse remains in the cavity until the desired amplification is built up. In ATLAS, after 13 roundtrips the pulse has gained an amplification of 10^7 up to an energy of 10 mJ. It is then switched out by the intracavity PC 2.

We calculated the pulse amplification in the RA by fractionizing the chirped pulse in a large number of small spectral packages which pass the amplifier one after the other as in reality. The amplifier is also partitioned in many segments. In each segment, one spectral package after the other is amplified. Each amplification process reduces the inversion slightly so that the later a spectral package runs through an amplifying segment the less gain it experiences. This effect is, of course, only present in case of saturation which sets in in the final round trips as can be seen from Fig. 13. The "pump" is the energy initially stored in the upper laser level. It is obtained from the actual green pump energy by multiplying this value with the absorption efficiency of 0.9, the quantum efficiency of 532/790 = 0.67, and the overlap factor between

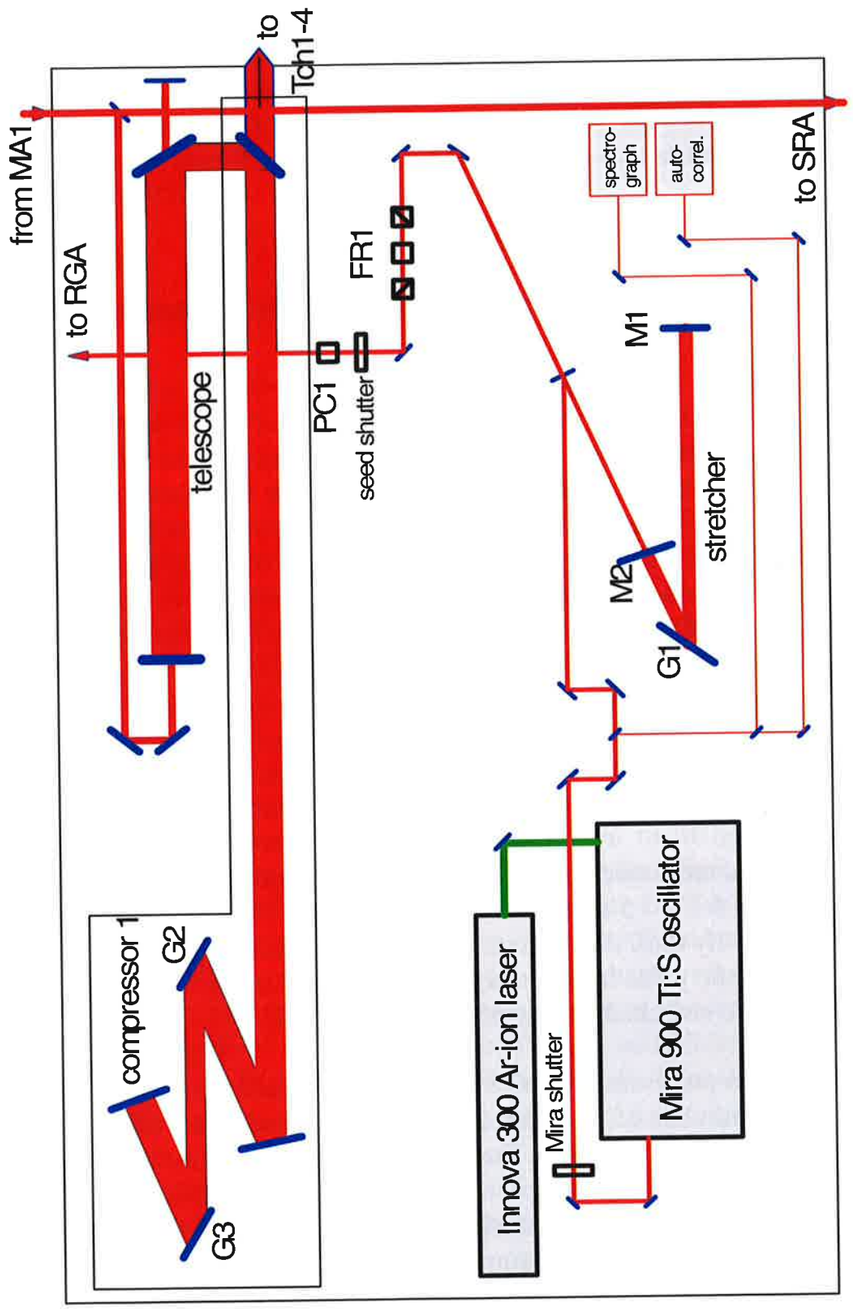

Fig. 12: ATLAS 2 with Mira-oscillator, stretcher and compressor; G1…3 gratings; M1,2 mirrors; FR1 Faraday rotator; PC1 Pockels cell; RGA regenerative amplifier; SRA superradiant amplifier; Tch target chamber.

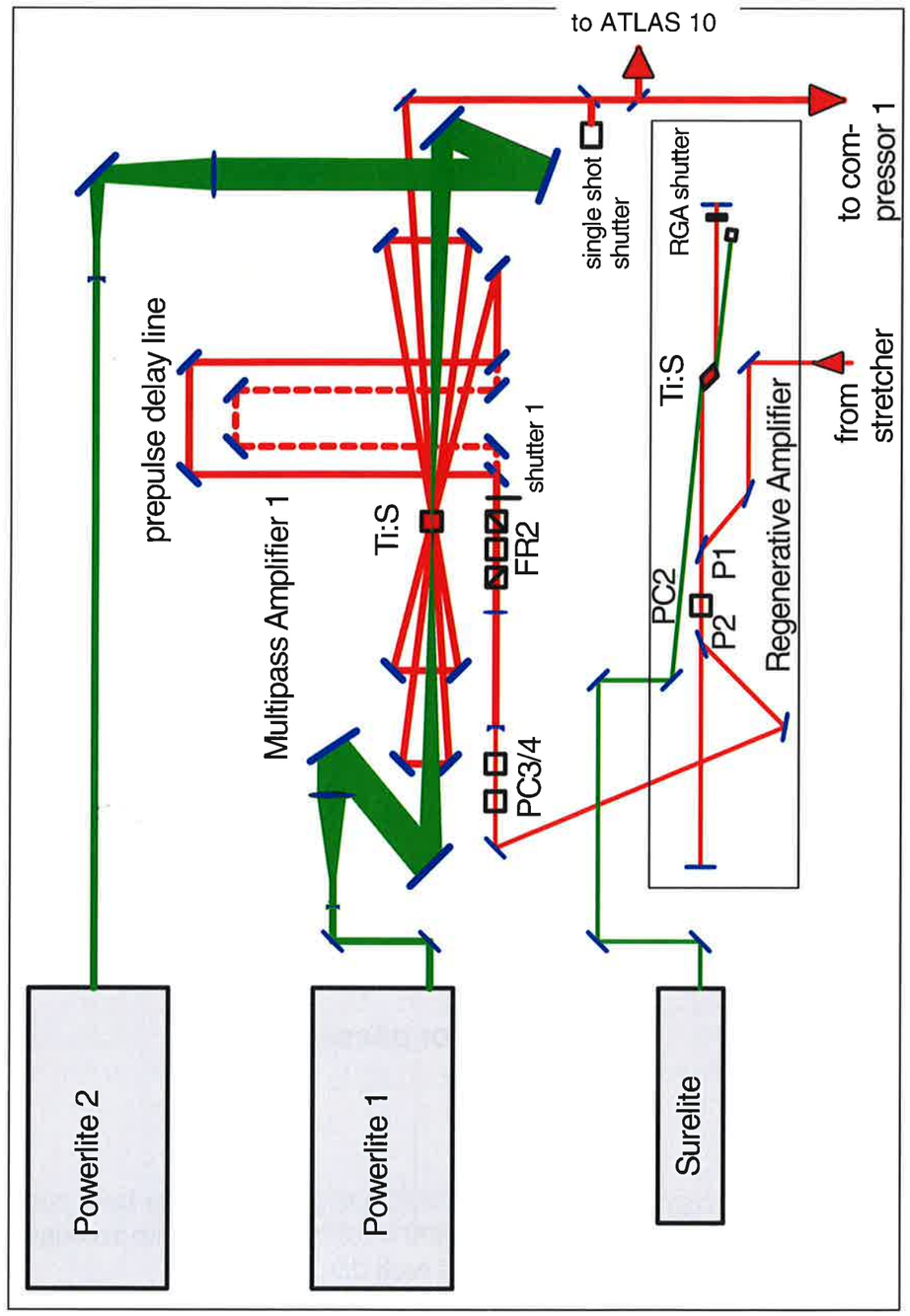

Fig. 12a: ATLAS 2 with regenerative amplifier RGA and multipass amplifier MA1; FR 2 Faraday rotator; P1,2 polarizers; PC3/4 Pockels cells.

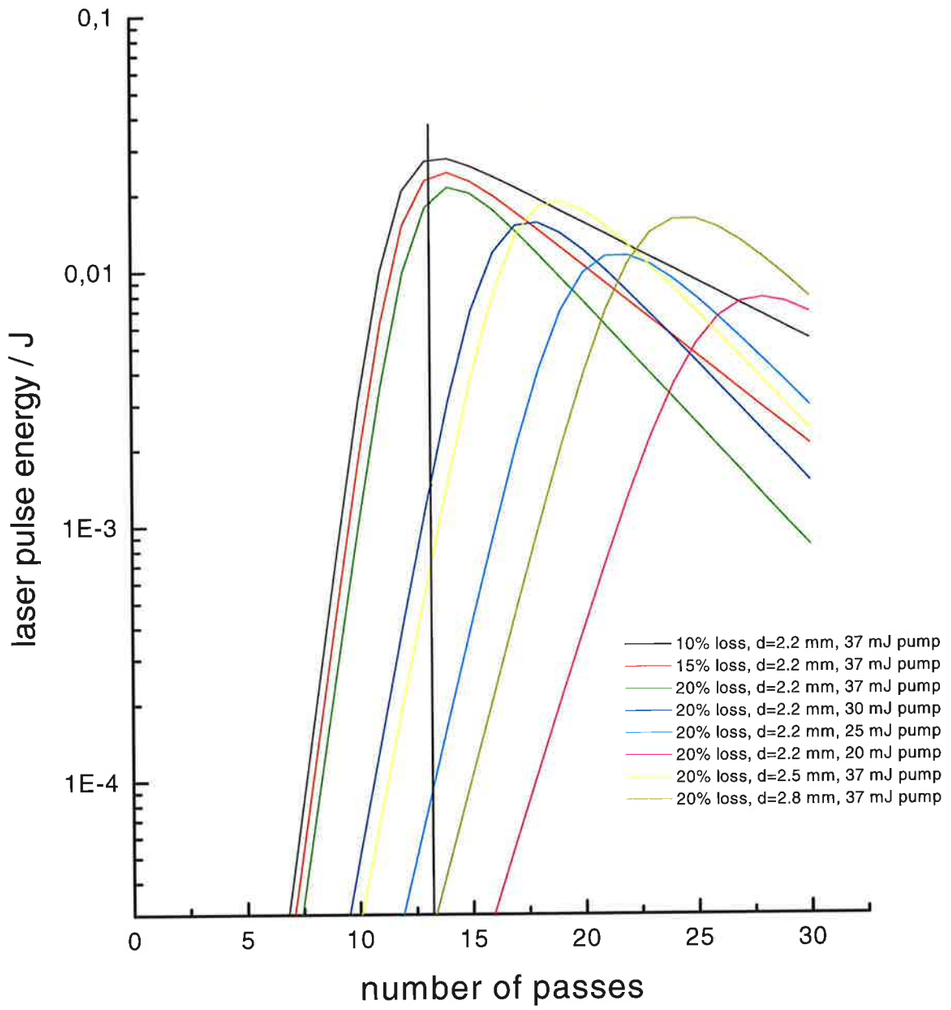

Fig. 13: RA output energy vs. number of passes; pump energy is 2ω-laser energy multiplied by the quantum efficiency of 532/790 = 0.67 and taking into account the beam overlap and the absorption efficiency of each 0.9.

pump and Ti:S pulse of ~ 0.9, altogether 0.55. The case with a pump slightly above 30 mJ and a 20 % loss yields an output energy close to that measured of 10 mJ after 13 round trips. The losses arise from the PC due to absorption and polarization mismatch as well as from the polarizers and the end mirror where the beam spot is smallest.

After a short time of operation, the HR-coating of this mirror gets slightly damaged. However, the damage turns out to be stable over long periods of time and stabilizes the transverse beam quality so that there is no need for an exchange. The associated transmission loss is ~ 10 %.

Fig. 14 shows the build-up of the pulse and the effect of the cavity damping. The pulse energy is limited by the damage of intracavity components. By a fast photodiode, a peak-to-prepulse intensity ratio of about 100 : 1 is measured, the prepulse being 12 ns before the main pulse, corresponding to one round-trip time.

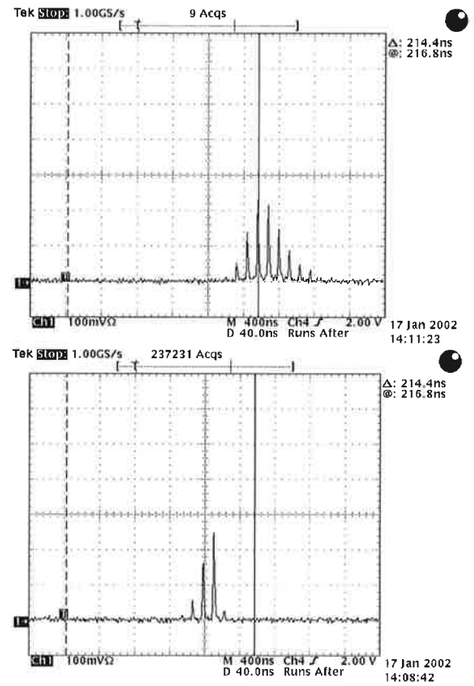

Fig. 14: Photodiode output during regenerative amplifier operation without and with cavity damping.

Two extra-cavity Pockels cells PC 3 and 4 and the associated Glan-Taylor po-

larizers are used to eliminate the pre- and post pulses that are reflected off the blocking polarizer with each round trip inside the cavity. With that, the peak-to-prepulse intensity ratio has been improved to better than 10^7.

The self-mode-locked Ti:S laser occasionally produces narrow spectral lines on top of the broadband spectrum of the pulses. These lines may correspond to pulses of tens of picosecond duration. This circumstance is a disaster for CPA, because these ps-pulses cannot be stretched to the duration needed before amplification and may lead to the damage of optical components. In order to prevent this, the firing of the pump lasers is controlled by an interlock system, which monitors the second-order spatially dispersed spectrum of the mode-locked pulses introduced by the stretching grating with the aid of a dual photodiode and prevents Q-switching when the bandwidth is too low for stretching the pulse to at least 150 ps.

Behind the RA we monitored a small red shift of about 2 nm of the pulse spectrum (see Fig. 16) which is explained in the next section.

4.2 Multipass amplifier 1

The output beam from the RA and the pulse slicers PC 3 and 4 is enlarged by a 3.6x Galilean telescope to 8-mm diameter. Then it traverses a second Faraday isolator which prevents the RA from back-reflected laser light and – on the way to the four-pass power amplifier 1 – it hits a mirror cabinet, which allows to generate a well-defined prepulse of 10 % of the main pulse energy and with a predelay time adjustable in-between 200 ps to 1.5 ns.

The Ti:S crystal of the MA 1 – produced by Crystal Systems with the heat exchanger method - is 18 mm in diameter and 15 mm long, having a 0.1 wt.% doping which corresponds to an absorption coefficient of α_{532nm}= 2 cm^{-1}, and AR coatings for both the 790-nm laser wavelength and the 532-nm pump laser wavelength on both faces. Two synchronized 10-Hz Q-switched Nd:YAG lasers, Powerlite 1 and 2 (see appendix A), pump the Ti:S crystal longitudinally from both sides with energies of 2 x 0.85 J; 95 % of that being absorbed in the Ti:S crystal. The pump beam profiles show spatial inhomogeneity which would be directly transferred to the amplified beam. Therefore it is essential to smooth the pump beam profile. A well proved method is smoothing by segmented integrating mirrors [18] which overlap different parts of the beam in the amplifier crystal (see Fig. 15), leading to an irradiance fluctuation smaller than 2 %. The Ti:S crystal is temperature stabilized to 20° and at the maximum pump energy density of 0.8 J/cm^2 only a black colour at the periphery is used to suppress self-oscillation perpendicular to the optical axis. The signal and pump beams propagate in a nearly collinear manner to maximize

the gain. About 25 % of the stored energy is thus extracted in 4 passes, which is in good agreement with modified Frantz–Nodvik calculations [19].

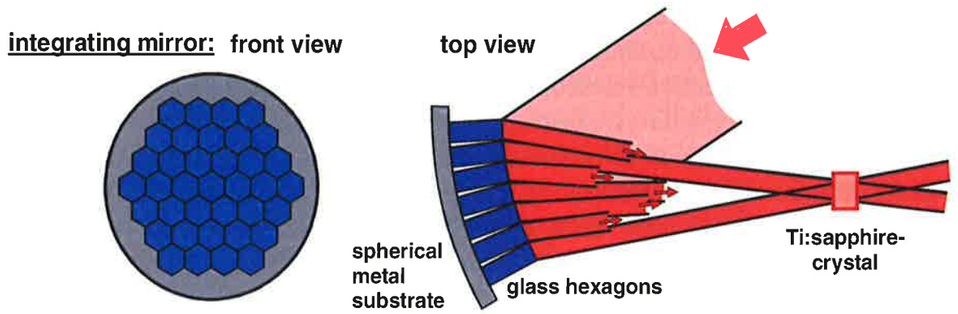

Fig. 15: Integrating mirror

As described in [2], we also monitored some narrowing of the spectrum and a spectral red shift of about 3 nm behind the MA 1 (see Fig. 16). This behaviour results from the fact that the red-shifted leading edge of the pulse experiences more gain than the trailing edge of the pulse. As a result, the central wavelength is slightly red-shifted and the spectrum halfwidth is somewhat narrowed.

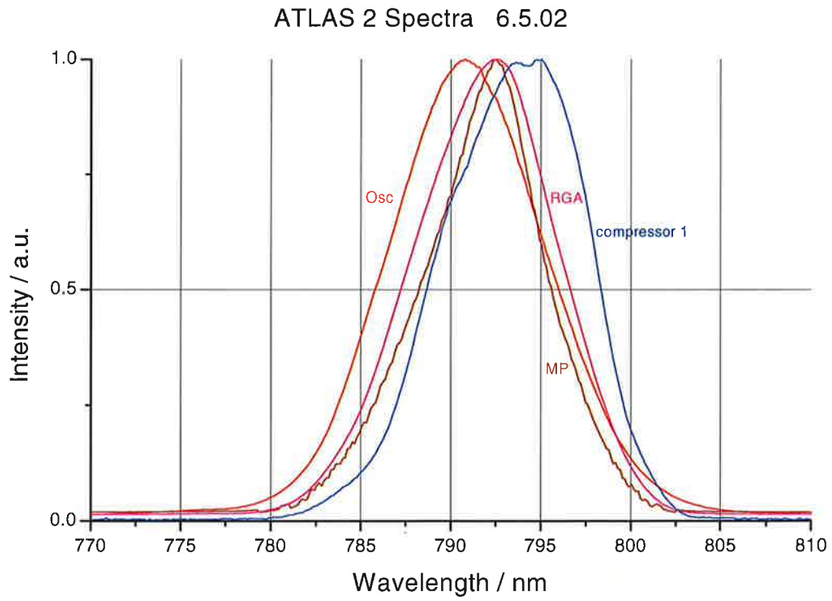

Fig.16: Pulse spectrum behind the oscillator, RGA, MA 1 and compressor 1

4.3 Pulse compression in ATLAS 2

After the amplification in MA 1 to energies up to 400 mJ, the laser pulses can either be directed to the multipass amplifier of ATLAS 10 for further amplification, or they can be compressed in the ATLAS 2 compressor. In the latter case, a 6.2x all-reflective telescope with spherical mirrors enlarges the laser beam to 50 mm diameter ($1/e^2$) in order to keep the fluence with 20 mJ/cm^2 approximately a factor of 10 below the damage threshold of the gratings. The pulse compression stage consists of a pair of gold coated holographic gratings from Spectrogon [20] with 1800 grooves/mm in a ruled area of 140 x 120 mm^2, and a HR dielectric mirror. Except for the size, the compressor gratings are the same as the stretcher grating and should be set at the same incidence angle, but now in a parallel formation (see Fig. 17) to delay the long-wavelength components.

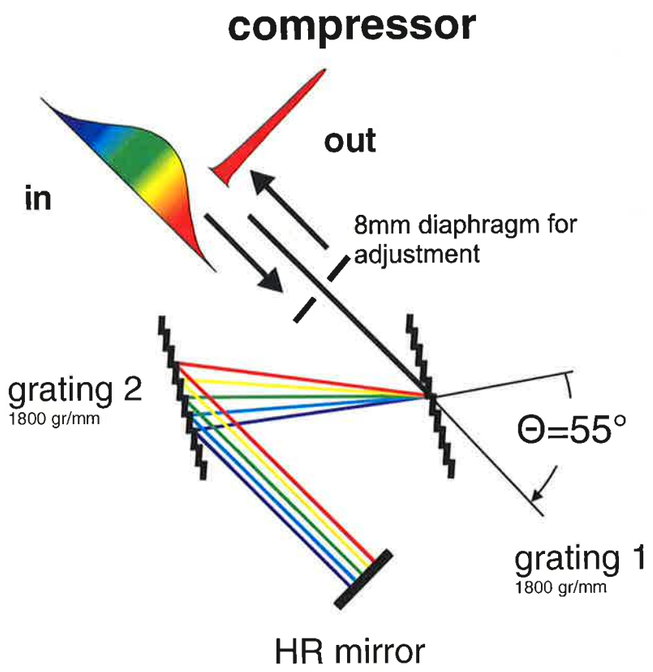

Fig. 17: Compressor scheme

However, because of the wavelength shift in the power amplifier and to compensate for linear dispersion in the optical material, the separation and the angle adjustment of the gratings have to be optimised in a special adjustment routine: The beam which is reduced to about 8-mm diameter using a centered

diaphragm is reflected back in itself by the first grating, giving the adjustment in the 0th order. Then this grating is rotated and adjusted until the first-order reflection is also centered on the diaphragm. Again one has to go to the 0th order and rotate by additional 55°, which is the angle of incidence in our case. Cover the HR-mirror and do the same procedure for both orders with grating 2, except that at the end it is rotated by 37.1° instead of 55°. In order to fine-adjust the parallelism of both gratings, the beam of a diode laser is directed to grating 1 in such a way that it is reflected 3 or 4 times from both gratings and that the reflections can be monitored sideways. Then grating 2 is slightly rotated until the distances between the reflections are equal. Afterwards the HR-mirror is adjusted such that the Ti:S laser beam can leave the compressor. Whilst this procedure has to be done at atmosphere, the ultimate fine-adjustment is done with remote handling when the compressor housing is closed and evacuated (in ATLAS 10) or filled with 1 bar He gas (in ATLAS 2). We monitor the following properties of the compressed laser pulse:
(i) Bandwidth with a spectrograph, (ii) duration with either a second- or third-order single-shot autocorrelator, and (iii) the pulse front tilt - which greatly influences the focus intensity - by using interferometric field autocorrelation [21]. The complete diagnostic system will be described in detail in section 7. A typical autocorrelation trace of the compressed pulses at 795 nm is shown in Fig. 18, delivering a minimum pulse duration of 120 fs when a sech^2 shape is assumed.

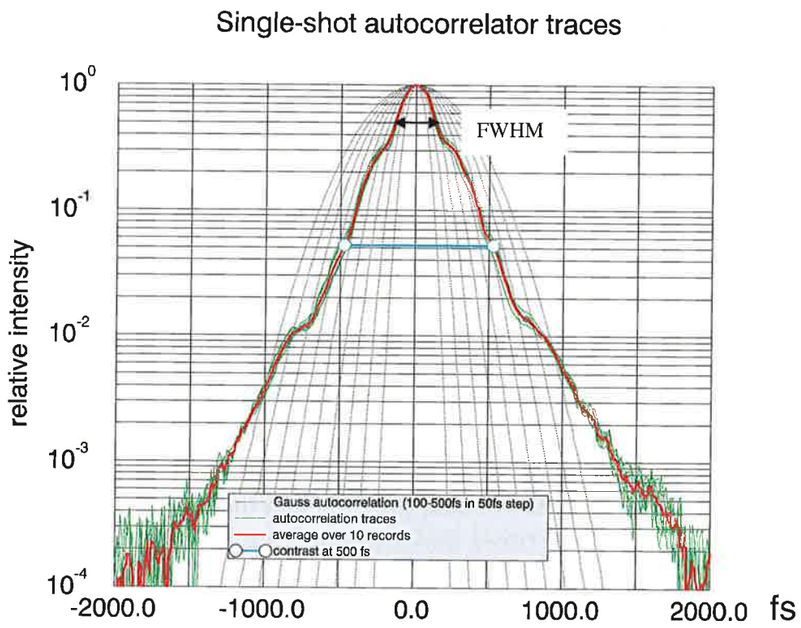

Fig. 18: Second-order-autocorrelation trace of ATLAS 2 pulse

The bandwidth of the compressed pulse is 8 nm, resulting in a time-bandwidth product of 0.456 showing that the compressed pulse is 1.4 times transform-limited for $sech^2$; for Gauss it is practically transform-limited. After amplification, Gauss is more likely than $sech^2$. The reflectivity of each compressor grating is 92 %, resulting in a total compressor transmission of 70 %. Hence a short-pulse energy of 280 mJ can be extracted whith a peak power of 2 TW. This value is the reason, why this ATLAS version is called ATLAS 2.

The contrast of the compressed pulse - defined as the ratio of the peak to background intensity - can also be deduced from the autocorrelation measurement to be better than 10^4 at 2 ps before the pulse peak. The long-term pulse-to-pulse energy fluctuations are smaller than ± 5 %. In order to avoid nonlinear phase distortion and beam degradation in air, the compressor is filled with 1 bar He. It should be mentioned that all optical components are mounted on a platform which is decoupled from the compressor housing, so that pressure changes do not impair the adjustment.

The spatial far-field beam quality is determined by focusing the attenuated beam with a long-focal lens in air or an f/3 off-axis parabolic mirror [22] in vacuum and measuring the focal spot with an 8- or 14 bit CCD camera in connection with an appropriate software. With the parabolic mirror, the 50-mm diameter beam can be focused to a spot of 15-µm diameter containing 85 % of the energy which corresponds to a peak intensity of $4 \cdot 10^{18}$ W/cm^2.

5. ATLAS 10: Pulse amplification and compression

5.1 Multipass amplifier 2

The output pulses from MA 1 of typically 300 mJ can be directed to a separate table on which the MA 2 of ATLAS 10 is installed (see Fig. 19). First, the super-Gauss beam profile is reduced from 13-mm diameter to 8 mm by a diaphragm in order to obtain a quasi top-hat profile. With that measure, the edges of the laser beam are truncated and the pulse energy is reduced to typically 220 mJ. Then a 2.25x telescope enhances the diameter to 18 mm and image relays the homogeneous beam profile from the diaphragm into the Ti:S crystal. A spatial filter of 5 times the diffraction limited diameter, i.e. 0.6 mm, cleans the laser beam from high frequency modulations [23].

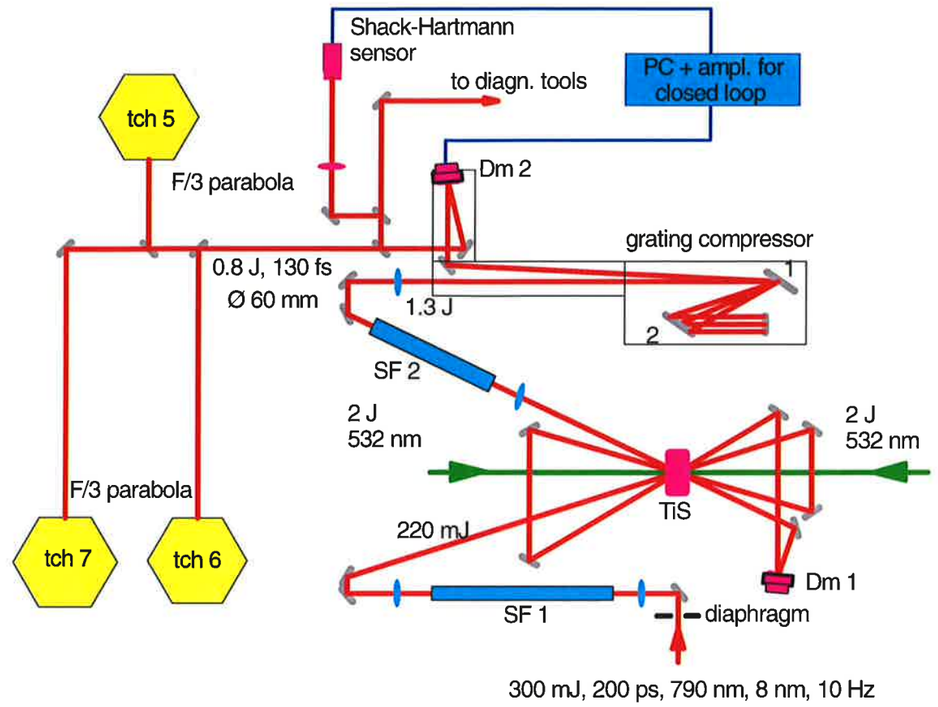

Fig. 19: Setup of the rear end of ATLAS 10

The principle of power amplification is the same as that in MA 1: A Ti:S crystal is pumped from both sides by 2 Q-switched, frequency-doubled Nd:YAG laser beams from a Powerlite 4 laser (see appendix B) and thus, the stored energy is extracted in part by the Ti:S laser pulse in 4 transits.

The dimensions of the Ti:S crystal are 40-mm in diameter and 17-mm length. It was produced by Crystal Systems applying the heat exchanger method [24] and is doped with about 0.08 wt.% Ti_2O_3, corresponding to a measured absorption coefficient of 1.58±0.02 cm^{-1} across the total area; 93 % of the 2 x 2 J pump energy are absorbed. Each pump beam diameter of 9 mm is enlarged to 90 mm by a 10x Galilean telescope and then focused to the Ti:S crystal via a segmented integrating beam homogenizer as described in ATLAS 2. The pumped area in the crystal is about 19 mm in a sexangle form and the resulting pump fluence amounts to 0.7 J/cm^2. The Ti:S crystal is temperature stabilized at 12° using circulating methanol and beyond it the housing is constructed such that the periphery of the crystal can be totally embedded in flowing 1 - Bromonaphtaline. Due to its high index of refraction of n = 1.66, this liquid is well suited for index matching (n_{790nm}= 1.76) in order to prevent

transverse self-oscillations that set on at a pump fluence of 1.2 J/cm^2 in absence of this measure. The entrance and exit surfaces of the Ti:S crystal are AR-coated for both the pump and the Ti:S laser beam utilizing the Solgel technique [25], featured by the highest available damage threshold as well as by the fact that it can be simply peeled off in the case of renewal.

From the absorbed pump energy of overall 3.7 J, the laser pulse can extract about 40 % at best and, consequently, the energy in the amplified laser pulse amounts up to 1.3 J after the fourth passage. As is the case in the RA and MA 1, our modified Frantz-Nodvik calculations can reproduce the experimental findings as to energy, spectral narrowing, and spectral shift. In MA 2, both spectral narrowing and spectral shift to the red turn out to be weak.

5.2 ATLAS 10 pulse compression

The amplified laser pulses pass a second telescope SF 2 which enlarges the beam from 18- to 63-mm diameter and image relays the Ti:S crystal to the short-pulse grating 1. The 5x diffraction-limited pinhole at the common foci site again suppresses high spatial-frequency modulations. Before entering the ATLAS 10 compressor, the pulse energy and the beam fluence are measured to assure that the damage threshold of the gratings is not exceeded.

There are two types of holographic, gold coated gratings with 1800 grooves/mm in operation: firstly the Spectrogon gratings with 140 x 120 mm^2 and identical to that used in ATLAS 2 and secondly, special manufactured gratings with 200 mm diameter from Lawrence Livermore National Laboratory. We have determined the damage threshold at 10 Hz and s-on-1 (i.e. many shots on 1 site) of both types to be 0.35 J/cm^2 for pulses of 200 fs and 0.5 J/cm^2 for 200 ps, respectively. Taking into account a safety factor for permanent operation of 3, the fluence in the laser beam must be below 0.12 J/cm^2, especially on the short-pulse grating 1. This means that the total pulse energy of 1.3 J can be transmitted through the compressor only when the fluence is very homogeneous. However, in practice we have measured an extremely modulated fluence with a peak of $\hat{e}$ = 0.3 J/cm^2 (see Fig. 20a) due to the fact that the Ti:S crystal shows serious growth defects (see Fig. 20b) and inhomogeneous thermal lensing when it is pumped.

The latter effect can be suspended by cooling the crystal to liquid nitrogen temperature [26], but, because of the technical effort, we will postpone it to the future. Currently, we compensate for both effects by using a deformable mirror [27] just before the last transit through the Ti:S crystal. With this, the

fluence in the plane of the short-pulse grating could be lowered from 300 to 90 mJ/cm^2 at 1.3 J input pulse energy (see Fig. 23), as will be described in detail in section 6.

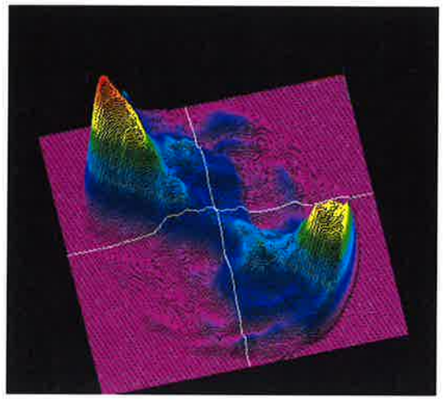

Fig. 20a: Fluence pattern at ATLAS 10 compressor gratings. The peak fluence is 300 mJ/cm^2.

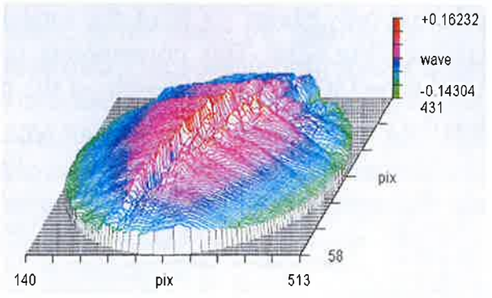

Fig. 20b: Interferogram of the TiS crystal in ATLAS 10 showing abrupt changes in the transmitted wavefront.

Not only the damage threshold of the gold coating is problematic, but also we recognized an epitaxial growth of carbon on the highly loaded sites of the short-pulse grating. This phenomena is well known from other experiments [28], too. The carbon layer is thought to arise from oil molecules cracked by the high-intensity laser pulses. In order to avoid this unwanted phenomenon, we take care of having as little oil molecules as possible in the compressor chamber by using oil-free vacuum pumps which produce a vacuum better than $3 \cdot 10^{-6}$ mbar. The better the vacuum, the less is the oil-vapour deposition rate.

The set up and adjustment procedure of the gratings is identical to that of ATLAS 2, as well as the diagnostic arrangement (see Fig. 28). At first the gratings are coarsely prealigned in air and then the fine tuning is done in vacuum. In this vein, the laser pulses can be optimised with respect to the shortest pulse duration of 130 to 140 fs and a pulse front tilted as small as possible in the near field which is a precondition for a high focal intensity [29]. The pulse energy at the ATLAS 10 compressor exit amounts up to 0.9 J, corresponding to a maximum power of 7 TW. With the originally envisioned pump energies of the Ti:S crystal of 2x2.5 J instead of the 2x2 J delivered presently and an even better homogenized beam, pulse powers of up to 10 TW are in reach.

6. Correction of wave front distortions and fluence profile modulations

The beam quality of ATLAS 10 comes off badly, mainly due to the afore mentioned problems associated with the Ti:S crystal. There is a substantial wave front distortion and, the associated focusability without any correction is such that only about 20 % of the total laser pulse energy is within the Airy disk (see Fig. 21). This corresponds to a Strehl ratio of less than 0.1, the Strehl ratio [30] S being the ratio of the peak intensity of an aberrated beam to that of a perfect beam:

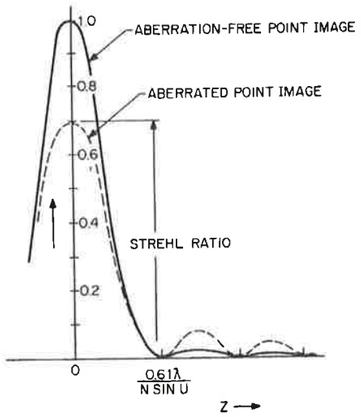

$$S = \frac{I_{peak}}{I_0}.$$

Fig.21: Strehl ratio

Normally the Strehl ratio can be improved considerably by using one deformable mirror in connection with a wave front measuring device, preferable a Shack-Hartmann sensor [31,32]. But in our case, the problem is manifold because of the presence of strong intensity modulations: In the near field, the fluence has to be homogenized and in the far field, i.e. in the focus of a mirror or lens, the Strehl ratio has to be brought close to unity by correcting the wave front. Both problems together can be accomplished only by the aid of *two* deformable mirrors.

As a consequence, we developed a corrective system using two deformable mirrors (DM) in close collaboration with the Adaptive Optics for Industrial and Medical Applications Group, IPLIT, Russian Academy of Sciences, Shatura, Moscow Region [33]. This group has rich experience with the production of DMs. It provided us with several DMs and wave front sensors, together with a sophisticated software to run the second DM in a closed loop [27].

The first DM smoothens the intensity profile in a region of a few meter length chosen far downstream from the mirror. The second mirror located in this region corrects the wavefront. In the following, it is shown how this novel concept is successfully implemented in the ATLAS beam line (see Fig. 19).

The first deformable mirror DM1 with an effective aperture of 30 mm and 17 electrodes arranged in two rings is placed in the beam line before the pulse makes the final transit through the amplifier. The second deformable mirror DM2 with an effective aperture of 80 mm and 33 electrodes arranged in three rings is incorporated into the beam line shortly after the compressor. Both mirrors carry a high-reflective dielectric coating with a damage threshold of 1 J/cm². Fig. 22 shows the construction of the bimorph mirror together with some typical data:

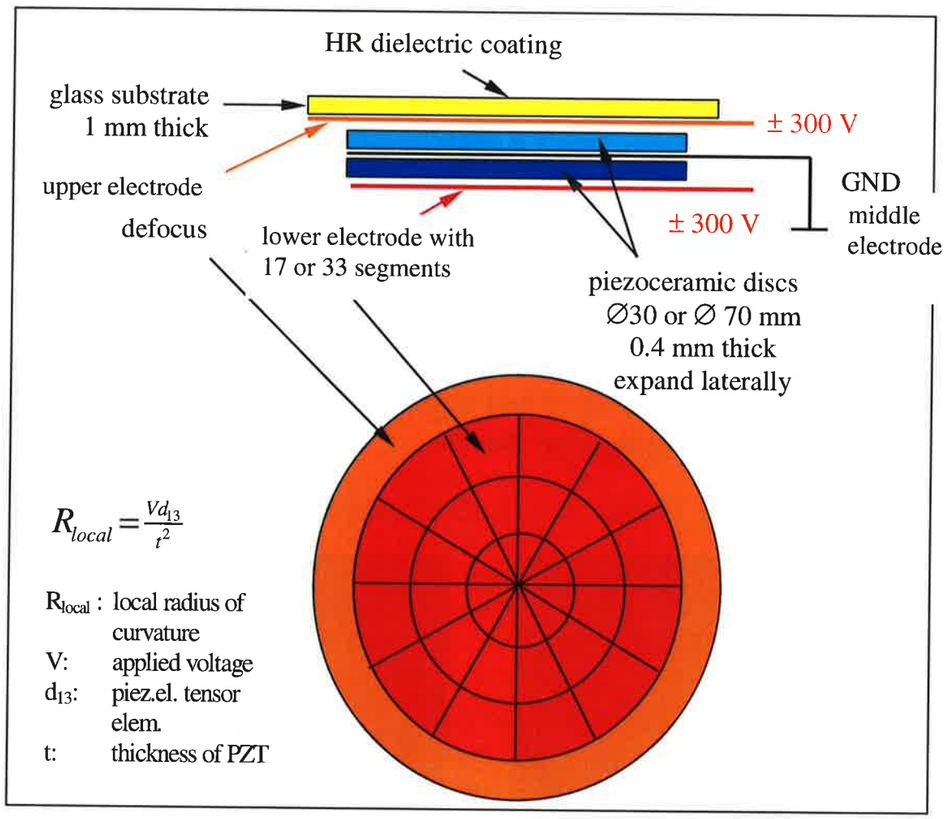

Fig. 22: Construction of deformable mirrors

A thin glass substrate with a HR dielectric coating is glued to an ensemble consisting of two piezo ceramic discs with coated electrodes on the upper and lower side and in-between (middle). When a certain voltage of up to ±300 V is applied, the piezos expand laterally and shrink whereby they locally bend with a radius of curvature which is directly proportional to the voltage V and the tensor element d_{13}, and inversely proportional to the square of the piezo thickness. Whilst the upper piezo is embedded in entire-surface electrodes (upper and middle) and therefore acts as a common focus or defocus element, the lower one has a structured electrode pattern on its outer side to correct for local phase distortions.

When a plane mirror is used instead of DM1, the fluence profile in the compressor is double-peaked (see Fig. 23a) with a maximal fluence of 300 mJ/cm² at a pulse energy of 1.3 J at the compressor entrance clearly proving the poor quality of the amplifying crystal. The pulse is largely freed from its highest spatial frequency components picked up in the crystal when passing the pinhole of SF2 whereby it suffers a slight energy loss. However, the peak fluence of 300 mJ/cm² is beyond the grating damage threshold of 150 mJ/cm² for long-term usage. The double-peaked fluence pattern would hence limit the compressor throughput to only about 500 mJ. When the plane mirror is replaced by DM1, the fluence profile in the compressor can be effectively smoothened (see Fig. 23b). It turned out that the best electrode voltage settings can be manually found by trial and error rather quickly. This reduces the peak fluence to 90 mJ/cm² so that the pulse can be safely transmitted through the compressor up to a maximal output energy of 1.3 J. The homogenized fluence profile remains stable over weeks at constant voltage settings of DM1. Inside the compressor and up to a few meters downstream, the smoothened profile remains rather similar.

Fig. 23: Fluence at ATLAS 10 compressor grating 1

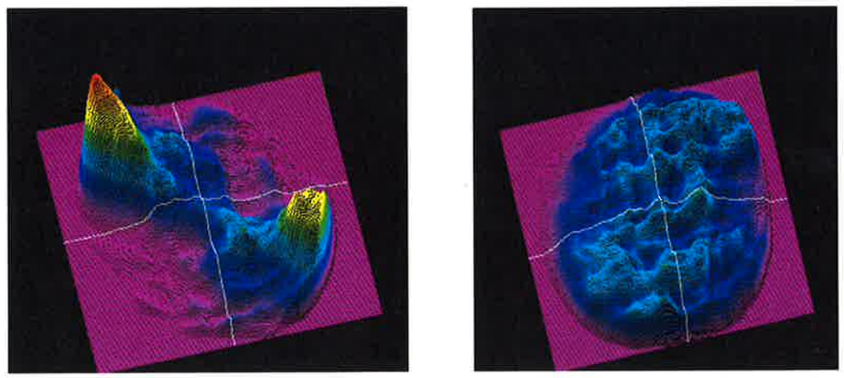

a: without DM1

b: with DM1 in operation

As already stated, the action of DM1 does not generate a plane wavefront in the compressor; the aberrations due to the amplifying crystal get, however, modified. Their cancellation is the task of DM2 which for safety reasons is best placed behind the compressor because then highly peaked intensity patterns which might occur during the optimization procedure of DM2 cannot damage the gratings. The compressor is hence fed with a chirped pulse having a distorted wavefront. In the following, we investigate the effects arising therefrom on the space-time characteristics of the recompressed pulse both analytically and by ray tracing. We show that the aberrations can be tolerated if certain conditions are met.

For the theoretical treatment, we replace the real pulse by a converging model pulse with a spherical wavefront of a curvature equivalent to the maximal local curvature occurring in the real distorted wavefront. Note that the passage of a convergent or divergent beam through a standard two-grating compressor run in double pass is a problem of general interest.

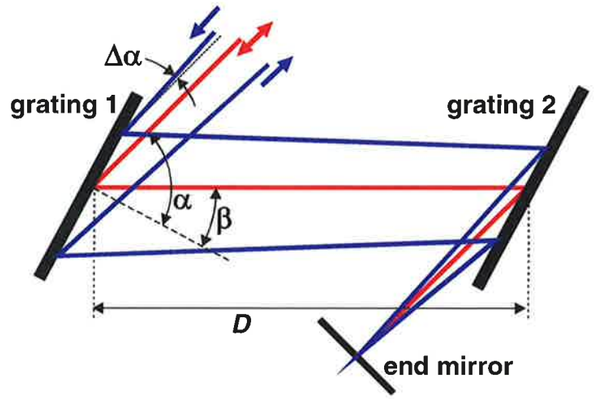

Fig. 24: Trajectory of a ray incident under the angle of α+Δα. The compressor is designed for the incidence angle α (red beam).

First we investigate the recompression of the convergent pulse. For this purpose, it is sufficient to consider a single ray having an angle $\alpha+\Delta\alpha$ (see Fig. 24) with the grating normal in the dispersion plane where α is the incidence angle of the central ray which the compressor is adjusted for: each ray entering the compressor under this angle in the dispersion plane leaves it by exactly running backwards the incoming path. We find that the relative uncompensable changes of the higher-order dispersion coefficients experienced by the tilted ray scale as $\Delta D_i/D_i = O\{1\}\cdot\Delta\alpha^2$ with $i=2,3,4$. There is no term lin-

ear in $\Delta\alpha$ because the corresponding contributions resulting from the first and second pass through the compressor cancel each other. This is a definite advantage of a double-pass compressor over a single-pass compressor. Since at ATLAS $\Delta\alpha$ is at most a few mrad, the pulse recompression is practically equal to that of a parallel beam. This also holds true for the non-dispersion plane (perpendicular to the dispersion plane). These deviations are too small to be experimentally verified since they are within the shot-to-shot fluctuations of the pulse-duration measurements of 130±15 fs.

Secondly, the originally spherically convergent beam turns astigmatic when leaving the compressor leading to the occurrence of two focal lines instead of a single point focus. This happens because the beam geometry is differently modified in the dispersion and non-dispersion planes of the compressor. The line-foci separation is independent on color and given by $2D\cdot[1-\cos^2\alpha/\cos^2\beta_0]$, where D is the oblique grating distance at α, $\beta_0=\arcsin(N\cdot\lambda_0-\sin\alpha)$ is the diffraction angle, N is the groove density of the grating, and λ_0 is the pulse center wavelength. The ratio of the line-foci separation to the average radius of curvature of the wavefront is a measure of the strength of the astigmatism. For a parallel beam, astigmatism is absent because the radius is infinite. For ATLAS, we have $D=67cm$, $N=1800$grooves/mm, $\lambda_0=790nm$, $\alpha=55°$, $\beta_0=37°$ leading to a line-foci separation of 65cm. From wavefront measurements taken at the compressor exit, we know that the local radius of curvature is always ≥15m. If a value of 15 m is assigned to the model pulse, the compressor-induced astigmatism turns out to be weak. It is easily correctable by a deformable mirror since the necessary surface displacement is ≤1 µm. The compensation of the original beam convergence is not a problem either.

Thirdly, chromatic aberration is also present behind the compressor because the path lengths of the individual spectral components through the compressor are different. Even though for each color the line-foci separation is the same as stated above thus allowing the cancellation of the astigmatism, the line-foci pairs of the individual colors do not fall upon each other but spread along the beam axis. Relative to the position of one of the two focal lines belonging to the spectral component at λ_0, the position of the corresponding focal line due to the wavelength $\lambda_0+\delta\lambda$ is displaced by $-2D\lambda_0N^2\delta\lambda/\cos^2\beta_0$. This phenomenon cannot be compensated by DM2. The beam emerging from DM2 will be parallel for the spectral components around λ_0, but divergent for the components with $\lambda<\lambda_0$ and convergent for those with $\lambda>\lambda_0$. When this beam is focused by the off-axis parabola, the focus is no longer point-like, but spreads out along the beam axis in form of a line since each spectral component has its own focus located at a different position. A criterion as to

the tolerability of this spreading is to require that the foci of all contributing colors for which we take those contained within four times the spectral FWHM, $\Delta\lambda$, lie within the Rayleigh length of the spectral beam component at λ_0. This happens when the local radius of curvature, R, of the aberrated wavefront upon entering the compressor meets the condition $2R>\pi\cdot d_{beam}\cdot\Delta\lambda\cdot(N/\cos\beta_0)^2$. The scaling of R with $\Delta\lambda$ is worth noting; very short pulses with a bandwidth of 50 nm or more need to be extremely well collimated in order to avoid intensity degradation in the focus. For ATLAS with $\Delta\lambda=8\ nm$, we have to meet $R>15\ m$ which is indeed the case as mentioned above.

We generate a parallel beam, i.e. a beam possessing a low wavefront distortion, with the help of DM2. This deformable mirror is actuated by a voltage pattern which is found by setting the voltages of the single electrodes such that the wavefront of the ATLAS 10 pulse matches a nearly perfect reference wavefront as closely as possible. Both wavefronts are measured with a Shack-Hartmann wavefront sensor (SHWFS) [27,31,32,33]. In the ATLAS 10 SHWFS a lenslet array is used which divides the laser beam in 20 x 20 beamlets and focuses it onto a progressive scan CCD-camera. A given wavefront distortion of the laser beam results in a deviation of the appropriate lenslet focus from the beamlet center and from all this focal positions the wavefront distortion can be recalculated. The reference wavefront comes from a diode laser running at 785 nm, its output is expanded to provide a beam of 63 mm diameter (the same diameter as the Ti:S beam) with a plane wavefront in interferometric quality.

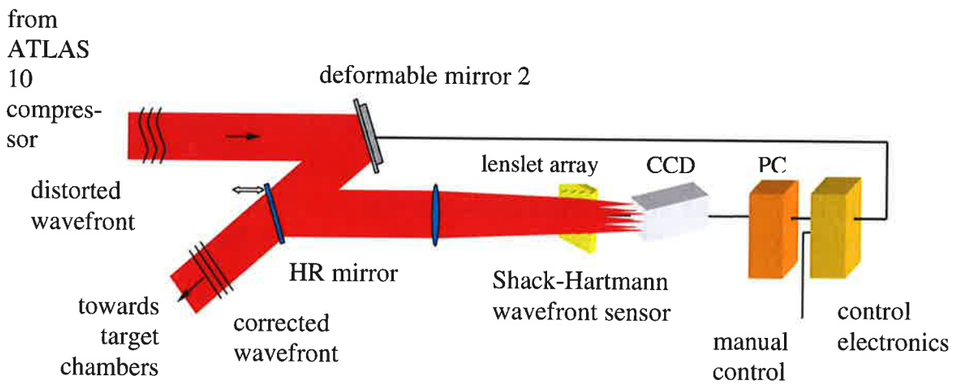

Fig. 25: Closed-loop for DM2

Because of the high thermo-mechanical stability of the ATLAS facility, the electrode voltage set can in principle be found manually by trial and error. It turned out, however, that it is not as easy as in case of DM1 but takes hours. We therefore realized the closed-loop solution (see Fig. 25). The algorithm which calculates the DM2 voltage settings needs the response functions of the 33 electrodes of DM2 as input. These are in-situ generated once only and then stored as an average over 10 laser shots; this takes about one minute. The deviations between the actual and reference wavefronts are minimized by repeatedly applying the least mean square fit. Usually, several ten iterations are needed which currently takes a few seconds. With this closed-loop operation, the peak-to-valley wavefront deformation could be reduced from originally 10λ to less than $\lambda/4$ (see Fig. 26). The voltage settings corresponding to minimal wavefront distortion are stored. They can be used for hours, because the shot-to-shot fluctuations of the wavefront remain small.

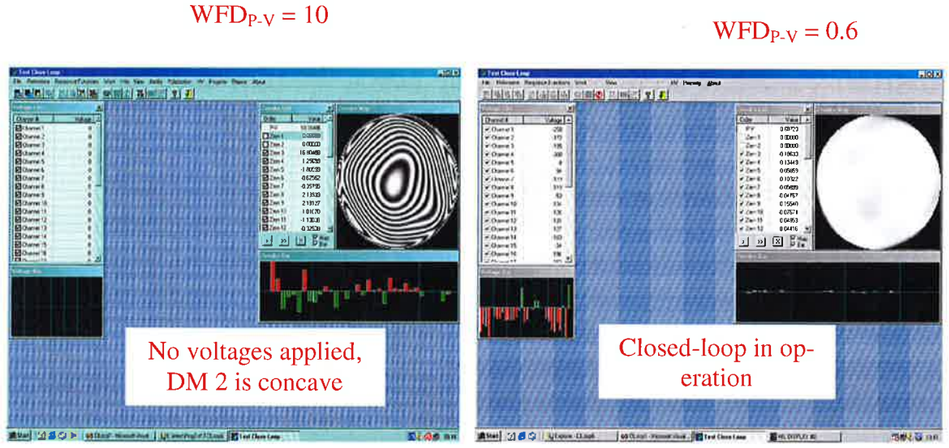

Fig. 26: Effect of closed-loop operation on wavefront

For routine operation of ATLAS, the beamsplitter feeding the Shack-Hartmann sensor has to be removed from the beamline in order to keep the B-integral low. In case of a deterioration, i.e. due to a thermal drift, the whole procedure beginning with the recording of the response functions has to be repeated.

We checked the quality of the corrected wavefront in each of the following three target chambers by measuring the fluence pattern in the focus of the f/3 off-axis parabola. In each case, we obtained the same result for thousands of shots. With DM1 turned on and DM2 operated to provide a plane surface, we find the multiple-peaked fluence pattern depicted in Fig. 27a. The Strehl ratio amounts to 0.1 only. When DM2 is, however, locked to operation for minimal wavefront distortion, we find a dramatic improvement as proven by Fig.

27b: A single peak appears, 65% of the pulse energy is contained within the diffraction limited diameter (DLD), the Strehl ratio climbs up to 0.8, and the mean intensity inside the DLD is raised by more than a factor of ten from ~10^{18} to $2 \cdot 10^{19}$ W/cm². The halo is attributed to high-order spatial frequencies still passing the pinhole of SF2 and not correctable by DM2.

Fig. 27: Focus of ATLAS 10 laser pulses

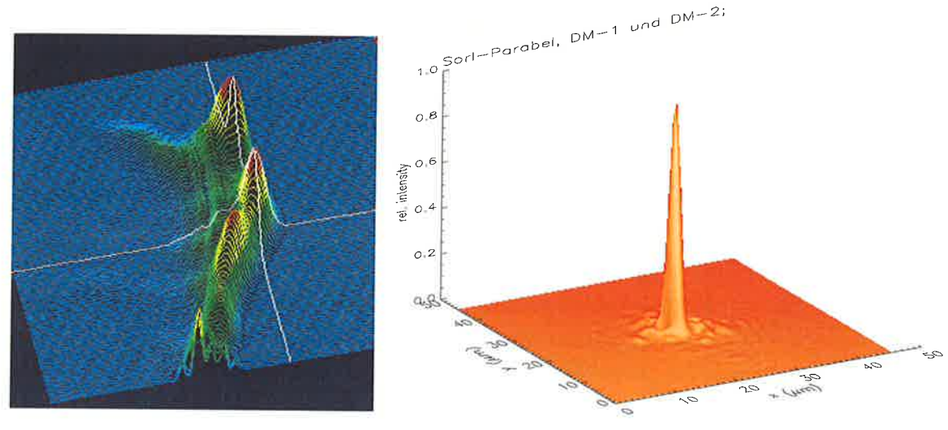

a: DM2 operating as plane mirror b: DM2 in operation with closed-loop

That the beam quality has indeed been remarkably improved is also corroborated by recently performed neutron experiments in which solid deuterium targets were irradiated with ATLAS pulses. We observed an increase in the neutron yield by almost two orders of magnitude when wavefront-corrected pulses were used.

We have shown that a combination of two deformable mirrors can free ultrashort laser pulses from simultaneously present severe wavefront distortions and strong intensity-profile modulations without any penalty in recompression fidelity.

7. ATLAS 2 and 10 diagnostics

For both ATLAS 2 and 10, we use similar sets of diagnostic tools but on different tables, which are placed near the particular beam exits. Fig. 28 shows the schematic arrangement of the ATLAS 10 diagnostic.

Behind the compressor 2 and the DM2, the laser beam in its full diameter of 63 mm is reflected to the diagnostic set via a HR mirror. It is possible to use

either the maximum pulse energy or about 1 % of it under the same pumping conditions of the Ti:S crystal by alternatively introducing a HR mirror or an uncoated BK7 glass wedge as turning mirror nearby the entrance of the compressor 2.

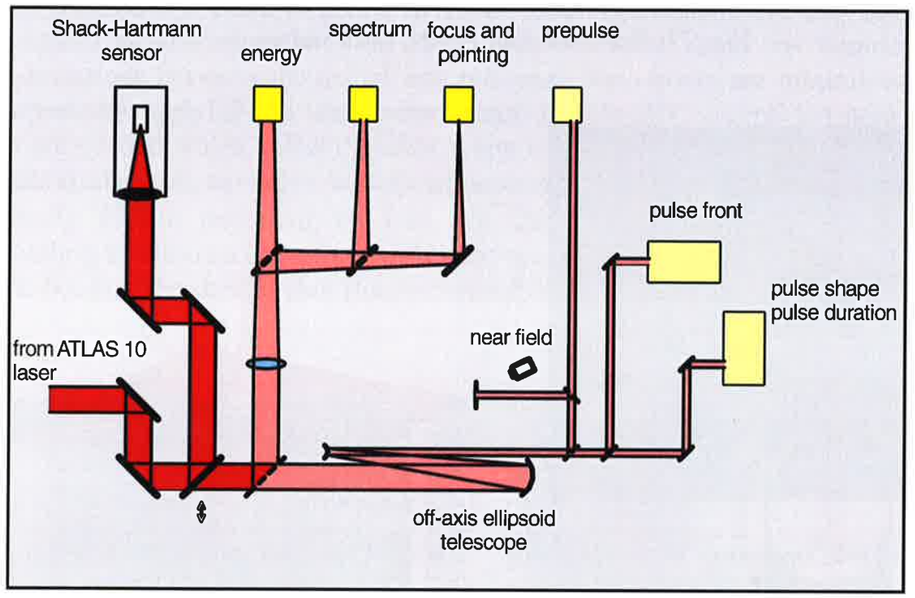

Fig. 28: ATLAS 10 diagnostic setup

Firstly, the beam can be directed towards the Shack-Hartmann wavefront sensor. Here, a single achromatic lens of 500 mm focal length reduces the beam diameter according to the dimension of the sensitive area of a CCD-camera. A lenslet array in front of the CCD splits the laser beam into 20 x 20 beamlets and focus these directly onto the CCD-chip. The position of the foci is a measure for the local wavefront distortion, this means that for a plane wave the foci are on axis of the beamlets and any deviation from the center can be recalculated to wavefront distortions. This information is used to improve the wavefront quality by applying the appropriate voltages to the electrodes of the DM2, manually or in a closed-loop as described above.

In a second branch, the full aperture beam is focused by a long focal length lens to a CCD-camera monitoring the quality and position, i.e. the pointing of the laser beam. In this branch, also the spectrum and the energy of the laser pulses are recorded, using an Oriel grating spectrometer and a calibrated pyroelectric calorimeter, respectively.

Afterwards the beam is reduced to 8-mm diameter by an all-reflective telescope composed of an off-axis ellipsoid mirror and a spherical one. With that, the near field pattern, the amount and time-scale of potential prepulses and ASE, the fore-mentioned pulse front and the pulse shape and duration are measured.

The ASE is monitored in a configuration consisting of two PIN-photodiodes (see Fig. 29 a). In ATLAS 2, two identical MRD 510 PIN-diodes are used for the detection of the main pulse and the ASE. In ATLAS 10, the main pulse is detected with a SFH 202 PIN-diode and the extremely overexposed AEPX 65 PIN-diode measures the ASE. Both signals are commonly displayed on a LeCroy digital oscilloscope 9362 with 1.5 GHz bandwidth. A typical measurement is shown in Fig. 29 c.

Using the main pulse and ASE signals as displayed by the oscilloscope, the energy and intensity contrast ratios of the ASE in reference to the main pulse can be estimated. Assuming that the areas under the ASE and main pulse voltages are proportional to the energy densities of the ASE, e_{ASE}, and the main pulse, e_{mp}, the following relations are obtained:

$$F_{ASE} \cdot e_{ASE} \cdot A_{d1} = a_1 \int U_{ASE}(t)dt \cong a_1 \cdot U_{ASE}^{\max} \cdot t_{ASE} ,$$

$$F_{mp} \cdot e_{mp} \cdot A_{d2} = a_2 \int U_{mp}(t)dt \cong a_2 \cdot U_{mp}^{\max} \cdot t_c .$$

F_{ASE} and F_{mp} are the filters used to appropriately attenuate the optical radiation. $A_{d1,2}$ are the diode areas and $a_{1,2}$ are constant factors representing the diode response to the received radiation. For the ASE energy contrast we find

$$\frac{e_{ASE}}{e_{mp}} = \frac{a_1}{a_2} \cdot \frac{F_{mp}}{F_{ASE}} \cdot \frac{A_{d2}}{A_{d1}} \cdot \frac{U_{ASE}^{\max}}{U_{mp}^{\max}} \cdot \frac{t_{ASE}}{t_c} .$$

Setting $e_{ASE} \cong I_{ASE} \cdot t_{ASE}$

and $e_{mp} \cong I_{mp} \cdot t_{mp}$,

where t_{mp} is the FWHM duration of the main pulse, we obtain for the intensity contrast

$$I_{ASE}/I_{mp} = \frac{e_{ASE}}{e_{mp}} \cdot \frac{t_{mp}}{t_{ASE}} .$$

a)

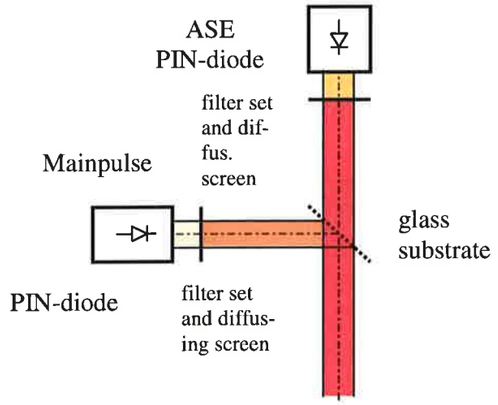

b)

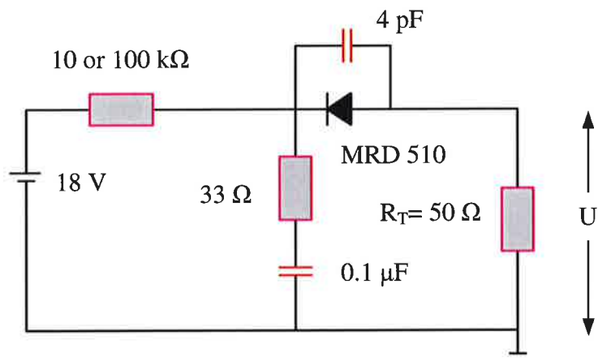

c)

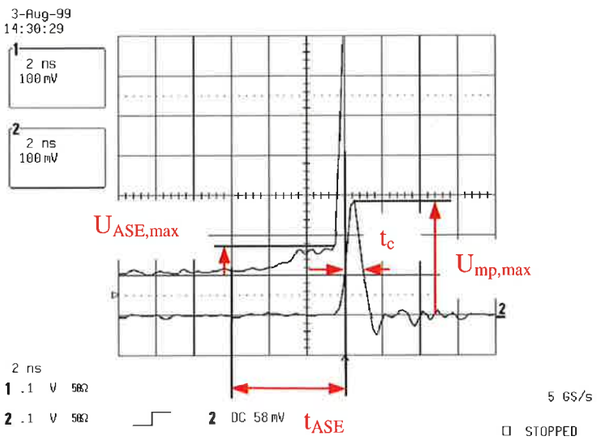

Fig. 29: a) Experimental setup for the simultaneous measurement of the main pulse and the ASE
b) Electrical circuit diagram
c) Oscilloscope display of the main pulse and ASE for ATLAS 2.

For ATLAS 2 we have (the following data are slightly different from that of Fig. 29c): $\frac{a_1}{a_2}\cdot\frac{A_{d2}}{A_{d1}}=1$ (identical diodes), $\frac{F_{mp}}{F_{ASE}}=2\cdot10^{-4}$,

$U_{ASE}^{max}/U_{mp}^{max}=\frac{350mV}{250mV}=1.4$, $t_{ASE}/t_c=\frac{6ns}{1ns}=6$, and $t_{mp}=120\,fs$ yielding

$\frac{e_{ASE}}{e_{mp}}=2\cdot10^{-4}\cdot1.4\cdot6\cong2\cdot10^{-3}$,

$\frac{I_{ASE}}{I_{mp}}=1.7\cdot10^{-3}\cdot\frac{1.2\cdot10^{-13}}{6\cdot10^{-9}}=3.4\cdot10^{-8}$.

For ATLAS 10 we have: : $\frac{a_1}{a_2}\cdot\frac{A_{d2}}{A_{d1}}\cdot\frac{F_{mp}}{F_{ASE}}=1\cdot10^{-3}$,

$U_{ASE}^{max}/U_{mp}^{max}=\frac{100mV}{280mV}=1.4$, $t_{ASE}/t_c=\frac{6ns}{1ns}=6$, and $t_{mp}=130\,fs$ yielding

$\frac{e_{ASE}}{e_{mp}}=1\cdot10^{-3}\cdot\frac{1}{2.8}\cdot6\cong2.1\cdot10^{-3}$,

$\frac{I_{ASE}}{I_{mp}}=2.1\cdot10^{-3}\cdot\frac{1.3\cdot10^{-13}}{6\cdot10^{-9}}=4.6\cdot10^{-8}$.

The low ASE level in both ATLAS versions is consistent with autocorrelation measurements which serve for measuring the main pulse leading edge over several orders of magnitude and the detection of prepulses. These can originate from misaligned optical elements, in particular the Pockels cell in the RGA and in the compressor when it is not properly adjusted. The prepulses might become as short as the main pulse. They cannot be tracked down by the slow ASE diagnostics. Hence a 3rd order autocorrelator is needed for their detection.

At ATLAS 10 a third-order autocorrelator was modified with a 2 m long delay line and coupled to a target chamber in order to detect these short pulses. The delay was varied in 5 cm steps and the autocorrelator was scanned over a 5 cm region for each step. Thus the whole 2 m delay range was sampled. In Fig. 30a these results are shown superimposed with the ASE measurement. This measurement show a large amount of prepulses at different times, e.g. leading to a strong preplasma formation. It was found that the source of these unwanted pulses was the too precise alignment of the Pockels cell inside the RGA perpendicular to the laser mode, so that the various crystal and window surfaces caused unwanted reflections of laser light into the mode volume of the RGA resonator, leading to a multitude of counter propagating pulses in the RGA with different round-trip times. Fig. 30b shows the temporal structure of the ATLAS 10 pulse after twisting the Pockels cell by a small angle.

a)

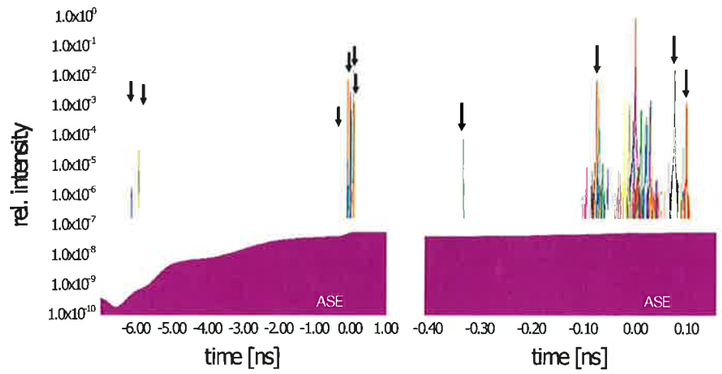

b)

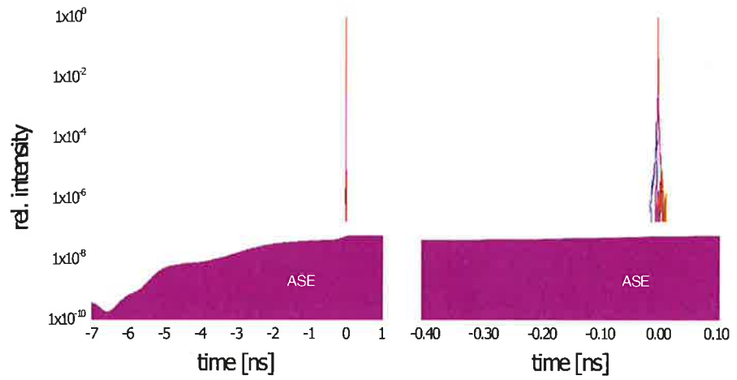

Fig. 30:
a) Short pre- and afterpulses as measured with the 3rd order autocorrelator for the whole delay range (left) and zoom into the last 400 ps before the main pulse (right). The real pre- and afterpulses are marked with arrows, others are measuring artifacts.
b) Prepulses removed by twisting the Pockels cell in the RGA. Only the main pulse remains.

For a rough estimate of the pulse shape, a 2nd order autocorrelator [21] (see Fig. 31) is sufficient. In this single-shot device, the laser beam is split into two equal parts using a beam splitter. Beam crossing is performed inside the KDP doubling crystal of about 1mm length at a small angle. The resulting 2ω signal is directed to a CCD linear detector and its fluence distribution gives the AC function. From that we get the information about the pulse duration and the intensity increase with time. Typically we find that within 1 ps before

the pulse peak the intensity raises by about 3 orders of magnitude (see Fig. 18). It should be mentioned that in the near future we intend to carry out this measurement with a fraction of the full beam diameter in order to obtain additional information about the pulse duration as function of the position across the beam.

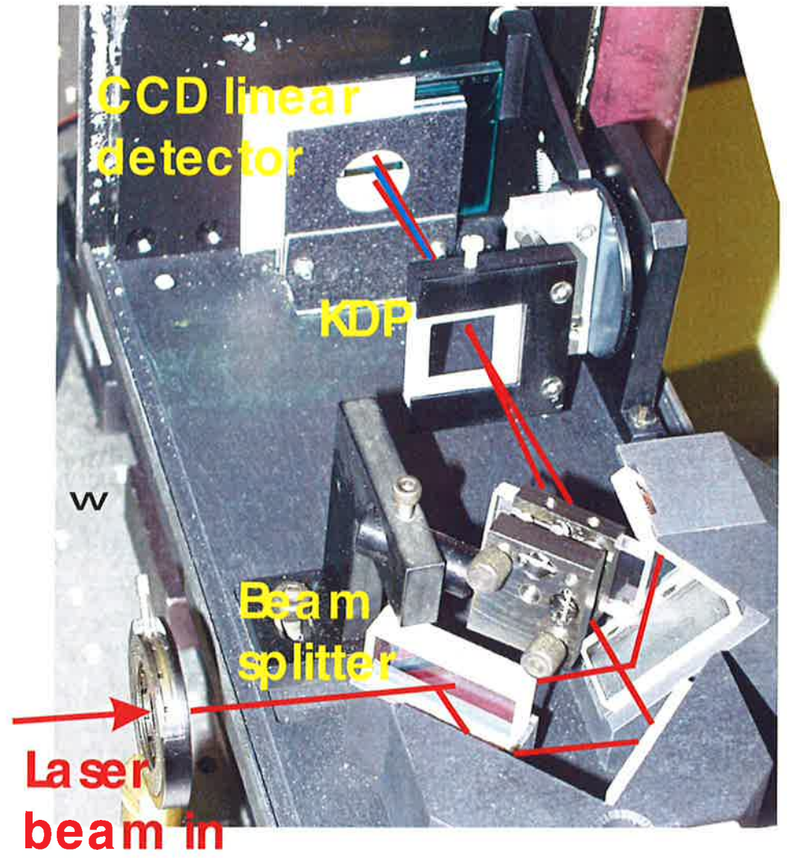

Fig. 31: Single-shot second-order autocorrelator

Angular chirp induced by slight parallelism-alignment errors in typical stretcher-compressor setups lead to tilted pulse fronts in the near field and a strong intensity reduction in the focus. Therefore it is essential to measure this angular chirp "live" and to minimize it by applying an exact alignment routine of the compressor. The pulse front can be monitored with the aid of an inverted field autocorrelator which delivers intuitive images and data for a quantitative evaluation, too. This device which was developed in our group and is described in detail in [29] is used routinely in both ATLAS versions .

In ATLAS 10, some additional diagnostics are installed, namely pyroelectric calorimeters to measure the pulse energies before the amplification in the Ti:S crystal and at the entrance of the compressor 2 and a CCD-camera to control the beam fluence profile in a plane equivalent to the position of the short-pulse grating. With this data, we are able to calculate the amplification in the Ti:S crystal and - what is more important – to watch that the peak fluence on the gratings is below the damage threshold.

8. ATLAS 50

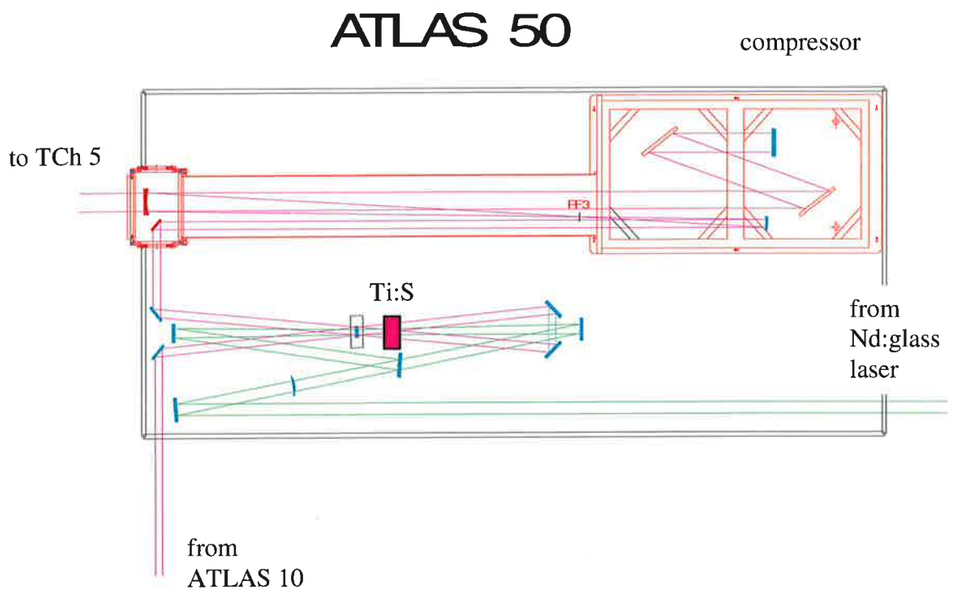

Fig. 32: ATLAS 50

ATLAS 50 (see Fig. 32) was constructed and built up in part in 1998. It is based on the experience we have made in 1996 when ATLAS 2 pulses were amplified directly in a 30-mm diameter Ti:S crystal pumped by 11 J / 3 ns pulses of a frequency-doubled Nd:glass laser (see appendix C). With it we obtained pulse energies of up to 2.8 J in 200 fs, corresponding to 14 TW. The pumping fluence of 1.7 J/cm^2 was high, but self-oscillation perpendicular to the beam axis could be suppressed using a high-refractive cooling liquid, namely 1-Bromonaphtalene. The penalty of this device was the low shot rate of only 1 shot per 10 minutes. In ATLAS 50 the Ti:S crystal is pumped by the same Nd:glass laser with the same low shot rate but with the difference

that now it follows ATLAS 10; that means that with the increased input energy of about 1.3 J the modified Frantz-Nodvik calculations predict an output energy of up to 5 J, which corresponds to a power of more than 30 TW. All components are ready to use, with the exception of the compressor housing.

9. Superradiant amplifier

9.1 SRA mechanism

Superradiant Amplification (SRA) is a novel amplification scheme for ultrashort laser pulses. The pulse is amplified in an underdense hydrogen or helium plasma while it is counter-propagating to a long pump pulse that delivers the energy (see Fig. 33). In other words: a portion of the long pump is compressed into the short signal pulse. The plasma is generated by ionizing the gas puff ejected from a pulsed nozzle. The ionization is effected by the leading edge of the pump pulse. The two pulses act on the plasma electrons in the interaction region such that they get arranged to form a density grid with a period of $(\lambda_{pump}\cdot\lambda_{sig})/(\lambda_{pump}+\lambda_{sig})$. The pump pulse is reflected partly from this structure by coherent Compton scattering. The reflection is similar to Bragg reflection. The coherence originates from the almost perfect bunching of the electrons at a single position within a grid period. Therefore all electrons see the same phase of the pump wave and radiate in phase. The density grid decays as soon as the signal pulse passes on and the backscattering ceases. Its transient nature prevents the signal from becoming longer. Instead the bunching process implies even a shortening while getting amplified. An input signal (seed pulse) of 25 fs and $\approx 10^{15}$ W/cm² will end with less than 10 fs duration and $> 10^{18}$ W/cm². Assuming that the cross section grows as well, an energy gain of more than 1000 appears to be possible. The necessary intensities of signal and pump and the plasma density scale with the laser wavelength. For a Ti:sapphire pump, the initial intensities are about $10^{15}..10^{16}$ W/cm^2 and the plasma density is 10^{18}-10^{19} cm^{-3}.

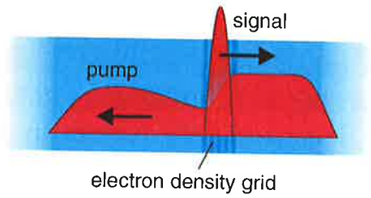

Fig. 33: Principle of SRA

Stretching and recompression of the signal, indispensable in any broadband laser medium for the amplification, is not necessary in the SRA scheme. Furthermore, high laser intensities will not cause any damage, since the plasma is already fully ionized and can withstand the invoked electric field strengths. Although the hydrogen or helium plasma has to be newly generated in each

shot, this material consumption is insignificant because of the low costs involved. These advantages may prove SRA to be a superior alternative to chirped pulse amplification on the way to highest powers for ultrashort laser pulses.

9.2 SRA experiment at MPQ

Our object is to implement SRA in our lab using ATLAS-2 as pump. In this first experiment, we aim to amplify the signal to 10-20 mJ. The pump has to be longer than the compressed ATLAS pulse, which is accomplished by detuning the compressor gratings. This way the pulse duration can be adjusted between 0.13 ps and 4.5 ps with an energy of up to 200 mJ. A major effort is the generation of the seed pulse. The SRA scheme requires its duration to be less than 30 fs, its intensity to be higher than 10^{15} W/cm² and a slight red shift in frequency with respect to the pump pulse. We consider different approaches to generate the seed pulse:
a) the hollow fiber compression technique,
b) generation and amplification of a whitelight continuum,
c) two-colour oscillator.

a) Hollow fiber compression technique

This approach is based on theoretical studies that showed that SRA should be also possible for non-detuned pump and seed pulses (see Fig. 34). In this case, the seed will be shifted in frequency during the first part of the interaction with the pump. The actual amplification will set in delayed. So the benefit of a simplified seed pulse generation is trade off by effectively reducing the amplification length.

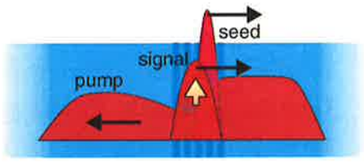

Fig. 34: SRA for non-detuned pump and seed pulses

For the hollow fiber compression technique [34], a small fraction of the ATLAS pulse is split off after the first multi-pass amplifier and is compressed in a separate compressor to 130 fs. To reduce its duration further, the spectrum has to be broadened, first. It is focused into a hollow fiber (∅ 250 µm) filled with Argon gas. While it propagates through the fiber, self phase modulation causes a large spectral broadening with a mainly linear chirp. The broadening depends on the fiber length, the gas pressure, and the pulse intensity. The proper adaptation of the focus to the fiber diameter and the alignment of the fiber in the propagation direction of the laser pulse is crucial to obtain a high transmission and a good quality of the transverse profile. For a high-grade

fiber one can achieve more than 60% transmission, an output energy of up to 1 mJ, and a perfect TEM_{00} mode profile after the fiber. Thermal drifts of the ATLAS laser make it necessary to realign the fiber from time to time. The pulse spectrum after the fiber has a width of more than 100 nm and looks quite jagged. Nevertheless, it can be compressed in a prism compressor to 20-30 fs and is ready as input for the SRA experiment.
One disadvantage of this compression technique is the moderate contrast ratio of the resulting pulses. Prepulse have intensities of 5-10 % of the main pulse and may cause problems for the SRA. Furthermore, the output spectrum is shifted somewhat to blue frequencies due to ionization effects which is opposite to what is favourable for the amplification.

b) Generation of a whitelight continuum and amplification of a spectral wave band

This scheme uses the generation and optic parametric amplification (OPA) of a whitelight continuum to create the short seed pulse. A small fraction of the main ATLAS pulse is split off and compressed to 130 fs. It is divided once more, the larger part is frequency doubled in a BBO crystal and provides the pump for the OPA. The tiny rest (≈1 µJ) is focused into a sapphire plate of 3 mm thickness, where it gets self-focused. The high intensity in the self-focusing channel leads to strong self-phase modulation. A continuum is generated which extends from 400 nm to 2 µm with a maximum at the original wavelength at 790 nm. The pulse has a mainly linear chirp and is several times longer than before. When it is now amplified by noncollinear optic parametric amplification (NOPA) in a BBO crystal [35], only a certain spectral band (30-40 nm) is amplified because of its linear chirp and because the whitelight is much longer than the frequency doubled pump pulse. One can select the center wavelength of the band by changing the delay between the whitelight and pump pulse. The resulting pulse is further amplified by a second NOPA stage or in a Ti:sapphire laser crystal which is pumped by a frequency doubled Nd:YAG laser. To avoid problems arising from the strong maximum of the whitelight, it is filtered with a RG850 glass. Finally a prism compressor will compress the pulse to 30 fs.

c) Two-colour oscillator for ATLAS

This version replaces the existing ATLAS oscillator with a two-colour oscillator (see chapter 2.3). It provides two Ti:sapphire pulses, which have independently adjustable duration and central wavelengths. But at the same time, they are synchronized on the fs-level by a coupling of the two laser cavities in the gain medium. One cavity is tuned to the specifications of the former ATLAS oscillator (100 fs, 790 nm) to feed the ATLAS amplifier chain. The

second cavity delivers 30-fs pulses at 830 nm. They are amplified in a non-collinear optic parametric amplification (NOPCPA) scheme, to reach the energy level necessary for the SRA experiment [36].

We have set up version a) and are currently implementing version b) and c).

9.2.1 Setup of the SRA experiment (see Fig. 35)

Having generated pump and seed pulses, their diameters are made equal to 25 mm by means of telescopes in order to have the same focusing parameters for the SRA experiment. The pulses are focused from opposite directions into a gas jet, where a plasma channel is created by the leading low-intensity part of the pump. It is a substantial problem of the experiment to prevent the pulses from running back the path of the other one after their interaction and causing damage to the ATLAS laser and the setup of the seed pulse generation, respectively. We use a combination of waveplates and polarizing beamsplitters to separate them. On both beamsplitters, the s-polarized signal is reflected and the p-polarized pump is transmitted. The λ/4 plates change the linear to circular polarization such that pump and signal have opposite polarization.

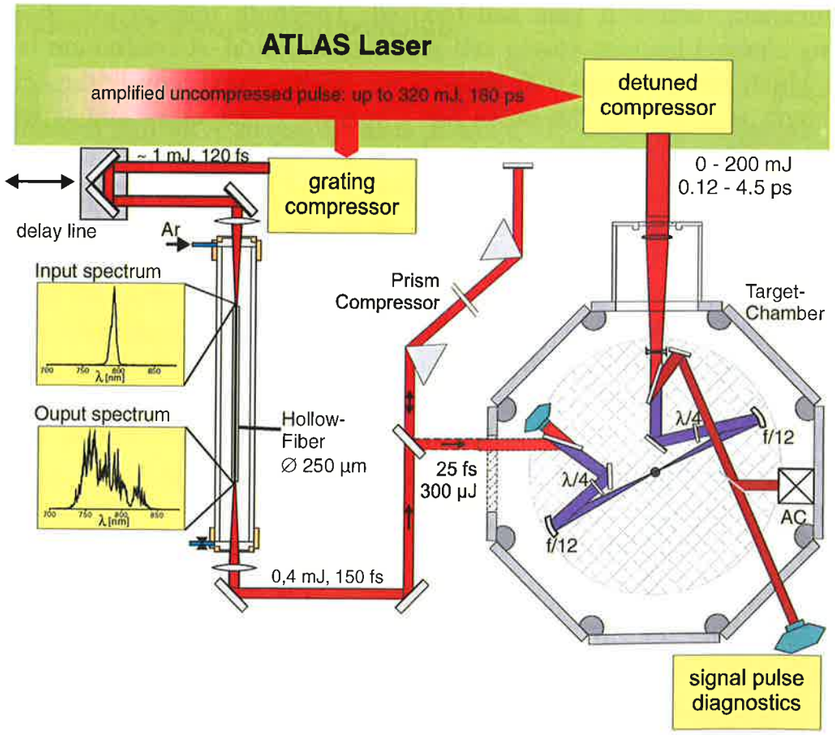

Fig. 35: Setup of the experiment using a hollow fiber to generate the seed pulse

This is the configuration required by the SRA mechanism. The passage through the second λ/4 reverts the polarization to the original one. Accurate alignment of the combination λ/4 plate and beamsplitter suppresses the pulses in the unwanted paths by 100 dB.

Another major difficulty is to ensure the overlap of the pump and signal focus in space and to match their arrival times in the gas jet. The latter is done using a streak camera. In the focal area, both pulses are reflected out perpendicularly to the entrance slit of the camera. By changing the length of a delay line, the temporal mismatch can be reduced to a few ps. The residual mismatch can be removed during the experiment by scanning the delay length to find the best temporal overlap for the amplification process. This is feasible because the width of the delay-gain curve is determined by the pump duration and the plasma length and lies on the ps-scale, too (see below).

To align the transverse position of the pump and signal foci (∅ 20 µm) a coarse adjustment is done by observing them on a screen in the focal plane by means of a telescope. For fine-tuning, a pinhole is used (∅ 20 µm), which both pulses have to pass. The longitudinal overlap is less problematic, because of the longer Rayleigh length of 800 µm. It is sufficient to do this once during the assembly of the experiment.

9.2.2 Experiment

For our first experiments, the seed pulse has been created with the hollow fiber technique. This means the frequencies of pump and signal are equal. The leading part of the pump pulse forms a completely ionized plasma along a channel in a H_2 or helium gas jet. We have set up diagnostics to analyze the signal output after the experiment. We measure its energy with an Ulbricht sphere and take the spectrum. To get information about the temporal profile, its autocorrelation trace is measured in a single shot device.

9.2.3 Experimental results

We started with reduced pump energy of 80 mJ and 1.6 ps pulse duration. Since the level of stimulated Raman scattering (SRS) increases with intensity and, most notably, with the pump duration, it is preferable to start with not too long pump pulses in order to be able to distinguish between the signal output and the Raman backscattered light. Figure 36 shows the dependence of the output energy on the delay between signal and pump. For the chosen energy and duration setting, the level of spontaneous SRS is well below the input signal.

The width of the amplification curve depends on the plasma length l_p, the Rayleigh length L_R, and the interaction length of signal and pump $c\tau/2$, where τ is the pump pulse duration. The orifice of the gas nozzle has a diameter of 500 µm, which is approximately the length, over which the plasma density is constant. The Rayleigh length is given by $L_R = \pi\omega_0^2/\lambda = 375$ µm, where $\omega_0 = 10$ µm is the radius of the focus. For $\tau = 1.6$ ps, the interaction length is 250 µm. The gain length is limited by the smallest of these values: $\min\{l_p, 2L_R, c\tau/2\} = 250$ µm. The amplification is maximal where both pump intensity and plasma density are highest $\min\{l_p, 2L_R\} = 500$ µm. The interaction may take place anywhere within this distance. Therefore, the amplification should be more or less constant for a delay range of (500 µm – 250 µm)/c = 1.6 ps, which corresponds to the width of the gain curve very well. The maximal energy gain is approximately 10. It does not drop to 1 on the left side where the seed arrives earlier, because the seed increases the noise in the plasma and thus enhances the SRS rate of the later coming pump.

Figure 37 shows the signal spectrum before and after the experiment. As expected, the amplification starts with the formation of a new signal pulse at the Raman-Stokes frequency of the pump pulse. Furthermore, a broadening at the base can be found, as it is predicted by simulations for the onset of SRA. To get beyond this early stage, a longer interaction length, i.e. a longer pump

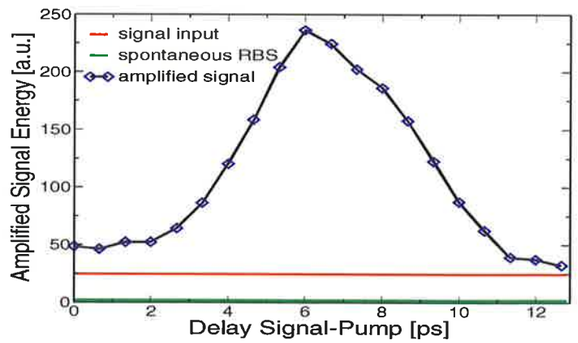

Fig. 36: Scan signal output vs. delay for a backing hydrogen pressure of 6 bar.

pulse duration, is needed. However, in experiments using pump pulses longer than 2 ps stimulated Brillouin scattering SBS sets in. This is a surprising result, because the minimal duration of pulses that are subject to SBS is expected to be several tens of ps. However, in our case the SBS was only observed when the seed pulse was injected, but not for the pump pulse alone. This means a 30 fs pulse can trigger SBS of a counter propagating ps pulse. The reason is that the pulses have the same wavelength, so that a resonant

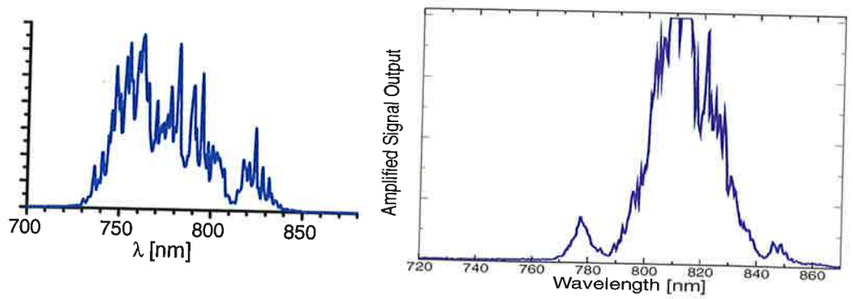

Fig. 37: Spectrum of the seed pulse (left) and the amplified output (right).

process becomes possible. To circumvent this problem, future experiments will be done with detuned pulses, i.e. the seed has a slightly lower frequency than the pump. The second parameter to be changed in the experiments was the backing pressure of the gas valve, which changes the plasma density proportionally. Figure 38 shows the output energy as function of the backing pressure. The data has been taken for the delay position, where the gain was maximal. The gain increases with plasma density. This is reasonable because a higher plasma density means that more electrons can participate in the scattering process. For higher pressures the output energies saturate, possibly because the plasma channel is not ionized completely anymore.

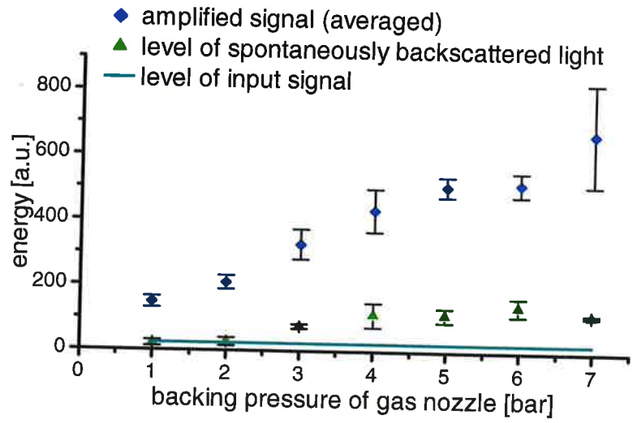

Fig. 38: Signal output energy as function of backing pressure

10. Target chambers and beam transport system

The ATLAS laser system can provide laser pulses to a variety of target chambers. ATLAS 2 is connected to 2 big and 3 smaller target chambers, whereas ATLAS 10 can deliver its pulses to three big ones. The target chambers (see Fig. 39) are quasi standardized in our group and besides a platform for the experimental arrangement they offer the possibility to add on a variety of diagnostics.

Fig. 39: Target chambers and beam transport system

Because of the high laser pulse intensity of up to $5 \cdot 10^{11}$ W/cm^2, an even low value of the nonlinear refractive index of $2.9 \cdot 10^{-19}$ cm^2/W for 120 fs pulses at 800 nm and atmospheric pressure [37] leads to a B-value of 12 when travelling 10 m through the laboratory. As outlined in the CPA section, already a B-value of 1 will have a dramatic impact on the beam quality. Therefore and in addition for safety reasons, we decided to transport the laser beam in a beam delivery system to the various target chambers which mainly consists of stainless steel tubes connected by special cubes. The complete system is mounted head-over and can be exhausted totally or in part to a residual pressure of p_{res} 10^{-4} mbar.

11. Single shot operation

Both ATLAS 2 and 10 can be operated with 10-Hz repetition rate or in single-shot mode. By far the most experiments are carried out with the 10-Hz repetition rate and in this regime the beam direction and pulse energy is stable within 2 hours at least. In contrast to that, we found that there is a difference in the behaviour when the ATLAS is adjusted in the 10-Hz mode and then switched to single-shot operation: The single-pulse energy is higher and the beam pointing changes. This behaviour is not fully understood, but it is related to the fact that in the 10-Hz mode the stored energy in the Ti:S-crystal of MA1 is regularly extracted, whereas in the single-shot mode it is extracted only from time to time by appropriately switching shutter 1 (see Fig. 12a) at the entrance of MA1. In order to overcome this fault, an additional single shot shutter (see Fig. 12a) is implemented behind the MA1 which – when shutter 1 is opened - allows a true 10-Hz operation in the MA1, but reflects the laser pulses to a beam dump until a reflecting mirror is opened fast to let only a single pulse pass. This operation mode has proved to be very valuable especially for direction sensitive applications like the SRA-experiments.

12. ATLAS electrical trigger scheme

As is shown in this report, ATLAS is a very substantial laser system with a variety of combinations of subsystems. That means that an integrative trigger circuit must coordinate the timing in different time scales beginning from the µsec-range, e.g. for flashlamp triggering down to the sub-psec-range for triggering Pockels cells or similar events with different requirements to the tolerable jitter. Fig. 40 shows the general trigger plan: It starts with the synchronization unit which phases the Mira pulses with the different laser functions in a 10-Hz mode via a central delay generator and appropriate trigger units and (HV-) pulsers. In doing so, the flash lamps, Pockels cells, thyratrons, Q-switches, and pulse selection systems of the Surelite, Powerlites and Nd:glass laser are triggered at the selected moments of time which is shown in Fig. 40 and 41. Besides this there are integrated several control functions like the bandwidth or back reflection monitor which can switch off the laser immediately in order to protect it from destruction. Another function is to provide trigger signals for diagnostic tools and for safety arrangements.

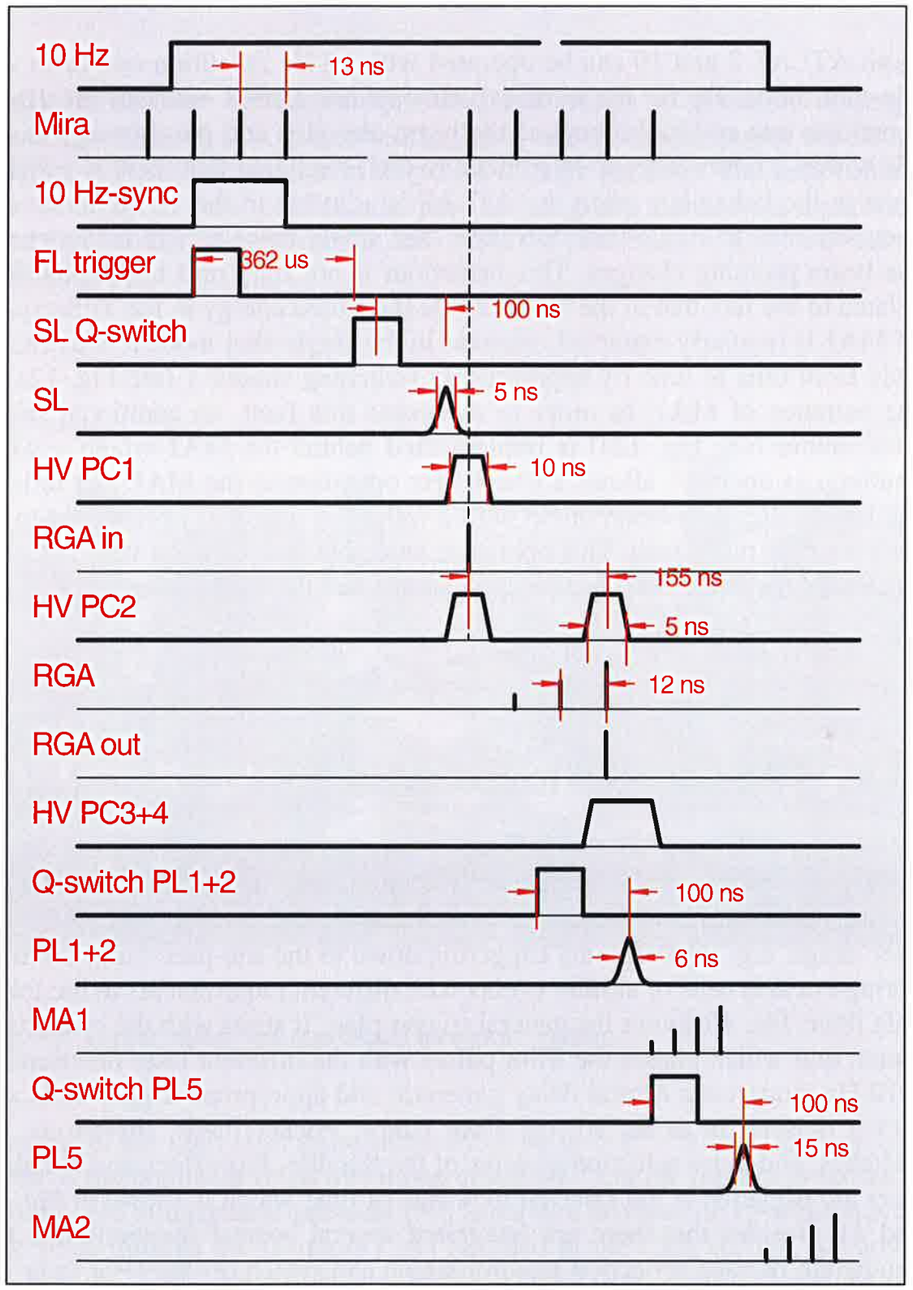

Fig. 40: Time schedule of trigger signals for ATLAS; abbreviations see Fig. 41

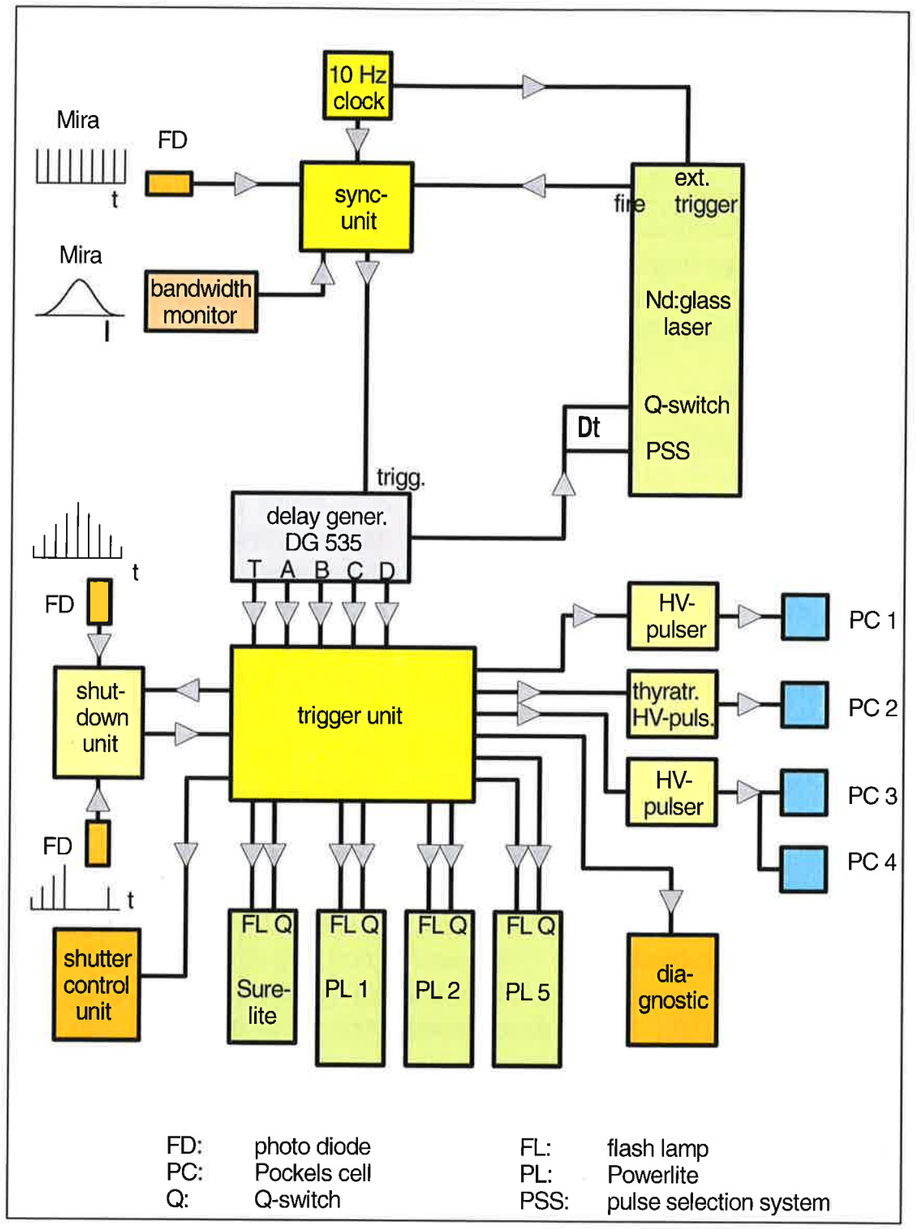

Fig. 41: Trigger scheme for ATLAS

13. ATLAS data

		ATLAS 2	ATLAS 10	ATLAS 50 (projected)
Pulse energy @ 793 nm	mJ	300	800	4000
@ 397 nm	mJ	100		
Pulse duration	fs	130	130	130
Pulse power	TW	2.3	6…8	30
Repetition rate	Hz	10	10	1sht/10min
Output wavelength	nm	793, 397	793	793
Focusability:				
energy in diffr. lim. diameter	%	65	65	65
Strehl ratio		0.8	0.8	0.8
fluence	W/cm^2	$4 \cdot 10^{18}$	$2 \cdot 10^{19}$	$6 \cdot 10^{19}$
Pointing stability	µrad	50	50	50
Ti:S crystal:				
Ø/thickness	mm	18/17	(30)40/17	(30)40/17
Ti_2O_3 concentration	wt.%	0.1	0.08	0.08
absorption @ 532 nm	cm^{-1}	2	1.57	1.57
Pumppulse @ 532 nm:				
pulse energy	J	2 x 1	2 x 2	2 x 6
pulse duration	ns	6	10	3
Deformable mirror		-	2	?

14. Summary

The ATLAS Ti:sapphire laser system is described in detail. It is a versatile work horse which delivers routinely laser pulses of up to 800 mJ in about 130 fs at 10 Hz. A single-shot version ATLAS 50 is constructed, which can deliver 4 J every ten minutes. The oscillator wavelength of 790 nm is redshifted to 793 nm behind the multipass amplifiers and, with the two-colour oscillator, a second wavelength between 810 and 850 nm is disposable in addition. For some experiments, e.g. in order to work with an improved contrast ratio, the pulses were frequency-doubled in KDP type I crystals with about 35 % efficiency. Investigations are en route to improve the efficiency by using type II crystals.

In ATLAS, three amplifiers are used: one of the regenerative and two of the multipass type. Here the Ti:S crystals are pumped by frequency-doubled Nd:YAG laser beams which were homogenized by simple segmented integrating mirrors. Nevertheless, but mainly due to crystal growth defects, the amplified ATLAS 10 beam quality is poor and needs to be improved by two deformable mirrors: whereas DM1 smoothens the two-peaked beam profile, DM2 corrects for the wavefront deformation in order to obtain the best possible focusability. Whilst for DM1 the optimal voltage pattern can be found by trial and error and, because of a high beam stability, can be maintained over several hours, DM2 with its 33 electrodes is operated in a closed-loop in conjunction with a Shack-Hartmann wavefront sensor. With the help of these measures, a maximum intensity of $2 \cdot 10^{19}$ W/cm^2 could be realized in ATLAS 10 and of $4 \cdot 10^{18}$ W/cm^2 without any corrective in ATLAS 2.

The beam pointing stability was measured to be about 50 µrad in both ATLAS versions, although the temperature drift in the laboratory is about 4° during a day. It is noteworthy that the ATLAS Ti:S laser system is about 9 hours a day in operation for experiments with a very high disposability of more than 95 % during a year.

Appendix A: Powerlite 1 and 2

Powerlite 1 and 2 are standard Nd:YAG lasers from Continuum, type 9010 which we use to pump the Ti:S crystal of MA 1 in ATLAS 2. They deliver up to 1 J at 532 nm in pulses of typically 6 ns duration at a repetition rate of 10 Hz. The opto-mechanical setup can be seen from Fig. 42.

Legend for PL9000 & 9030

1. Mirror, rear, (rep rate dependent)
2. Pockels cell, 202-0001
3. λ/4 plate, 108-0001
4. Dielectric polarizer, 199-0116
5a. 811U-06 head, 506-3500
(for 10, 20 & 30Hz)
rod, 6mm, 201-0056
flashlamp, 203-0019
5b. 811U-05 head, 506-9050
(for 50 Hz)
rod, 5mm, 201-0094
flashlamp, 203-0019
6. Output coupler, (rep rate dependent)
7. Mirror, turning, 45°, 105-0002
8. Div. lens, -104mm, 102-0005
9. Con. lens, +155mm, 101-0001
10. λ/2 plate, 108-0004
11. Apodizer, 110-0004
12. Pinhole
13. 811U-09 head, 506-2800
rod, 9mm, 201-0005
flashlamp, 203-0036
14. Dichroics, 532nm, 105-0022
15. Dichroics, 1064nm, 105-0002
16. Mirror, turning, 30°, 105-0086
17. Dielectric polarizer, 199-0055
18. Dichroics. 355nm, 105-0023
or 266nm, 105-0025
19. Div. lens, rep rate dependent
20. Rotator, quartz, 199-0067
21. 811L-09 head, 506-2700
rod, 9mm, 201-0005
flashlamp, 203-0036

For PL9050 layout, see page facing 2-1.

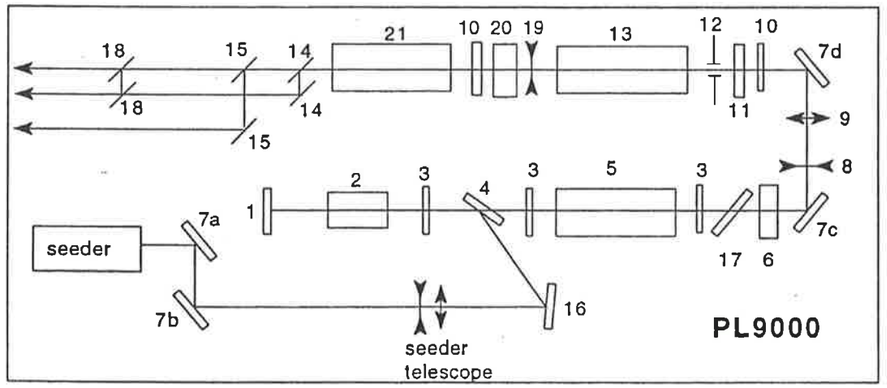

Fig. 42: Powerlite 1 and 2

Appendix B: Powerlite 4

Powerlite 4 is a Nd:YAG laser which Continuum has developed especially for pumping Ti:S crystals. The temperature stabilized oscillator is seeded by a diode laser thus delivering smooth pulses between 3 and 15 ns duration. The pulse energy is enhanced in two common amplifiers and - after the beam is splitted – in 4 consecutive amplifiers in each leg up to 5 J at 1064 nm. Then the pulses are frequency doubled providing an output energy of up to 2.3 J at 532 nm in each beamlet with a repetiton rate of 10 Hz, but the routinely usable pulse energy amounts less than 2 J. The arrangement is shown schematically in Fig. 43.

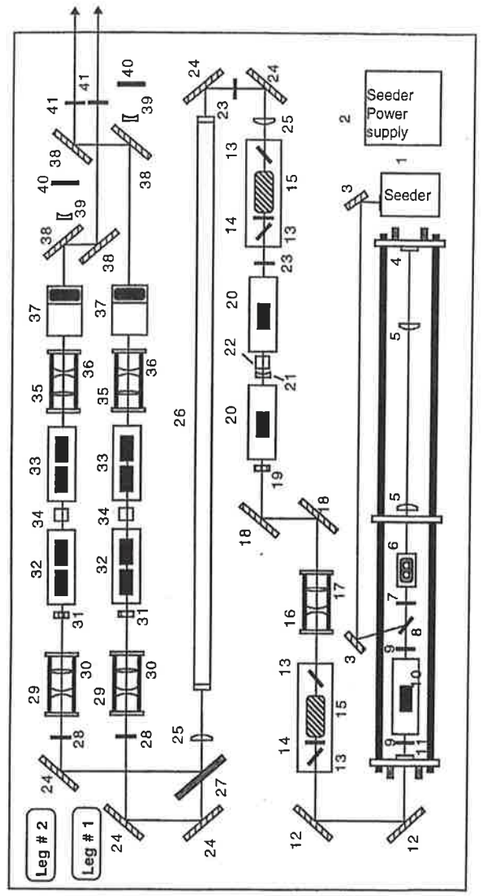

Legend for custom long pulse system

1. Lightwave seeder, 299-0022
2. Seeder power supply, 299-0023
3. 90° turning mirror for 1064nm, 105-0002
4. 4m HR mirror @ 1064nm, 104-0026
5. Lens, +250 AR @ 1064nm, Custom51
6. Pockels cell, 202-0001
7. Quarter-wave plate for 1064nm, 108-0001
8. Dielectric polarizer, 199-0055
9. Quarter-wave plate for 1064nm, 108-0001
10. 811U-06 head
rod, 6mm, 201-0056
flashlamp, 203-0019
11. 10 Hz Gaussian output coupler, 104-0020
12. 90° turning mirror for 1064nm, 105-0002
13. Dielectric polarizer, 199-0055
14. Half-wave plate for 1064nm, 108-0004
15. Faraday rotator, 12mm clear aperture, 199-0099
16. Lens, -120 AR @ 1064nm, 102-0007
17. Lens, +155 AR @ 1064nm, 101-0001
18. 90° turning mirror, 31mm @ 1064nm, 105-0007
19. Pinhole, 8.5mm, 314-0177
20. 811U-09 head
rod, 9.5mm, 201-0005
flashlamp (1), 203-0036
21. Lens, -3000 AR @ 1064nm, 102-0015
22. Quartz compensator, 199-0067
23. Half-wave plate for 1064nm, 108-0004
24. 90° turning mirror 31mm @ 1064nm, 105-0007
25. Lens, +1000 AR @ 1064nm, 101-0069
26. Vacuum tube (L=165cm or 65"), Custom 20
27. 2" beam splitter, R~50% T~50% @ 1064nm, 105-0120
28. Half-wave plate for 1064nm, 108-0004
29. Lens, -150 AR @ 1064nm, 102-0044
30. Lens, +200 AR @ 1064nm, 101-0074
31. Soft aperture AR@1064nm, ~ 11mm
32. 812H-12 head (horizontal head), 507-0950
rod, 12.7mm, 201-0057
flashlamps, 203-0032
33. 812V-12 head (vertical head), 507-0970
34. Quartz compensator, 199-0067
35. Lens, +200 AR @ 1064nm, 101-0074
36. Lens, -150 AR @ 1064nm, 102-0044
37. Type II KD*P doubler, 30mm long, 5/8", 635-0350
38. 1" dichroic mirror with adaptor ring, 105-0022 & Custom 65
39. Lens, -150 AR @ 1064nm, 102-0044
40. Ceramic beam dump, 314-0277
41. Half-wave plate for 532nm, 106-0003

Fig. 43: Powerlite 4

Appendix C: Nd:glass laser

Since 1992, we use the Nd:glass laser from Continuum for a variety of target experiments and, in addition, to pump Ti:S crystals in order to enhance the Ti:S pulse energy, e.g. in ATLAS 50. The Nd:glass laser uses a seeded oscillator which delivers - together with the pulse cutting system - smooth pulses between 3 and 15 ns. The pulse energy is raised in consecutive Nd-YAG and Nd:glass amplifiers (see Fig. 44a and b) up to 35 J at 1064 nm. After frequency-doubling, single pulses with energies of up to 13 J at 532 nm are provided. Because the last 3 amplifiers with 16, 25, and 45-mm diameter use Nd:glass as the active medium, the pulse repetition rate is restricted to 1 shot per 10 minutes only. A sophisticated triggering scheme (see Fig. 40, 41) integrates the Nd:glass laser to the ATLAS system.

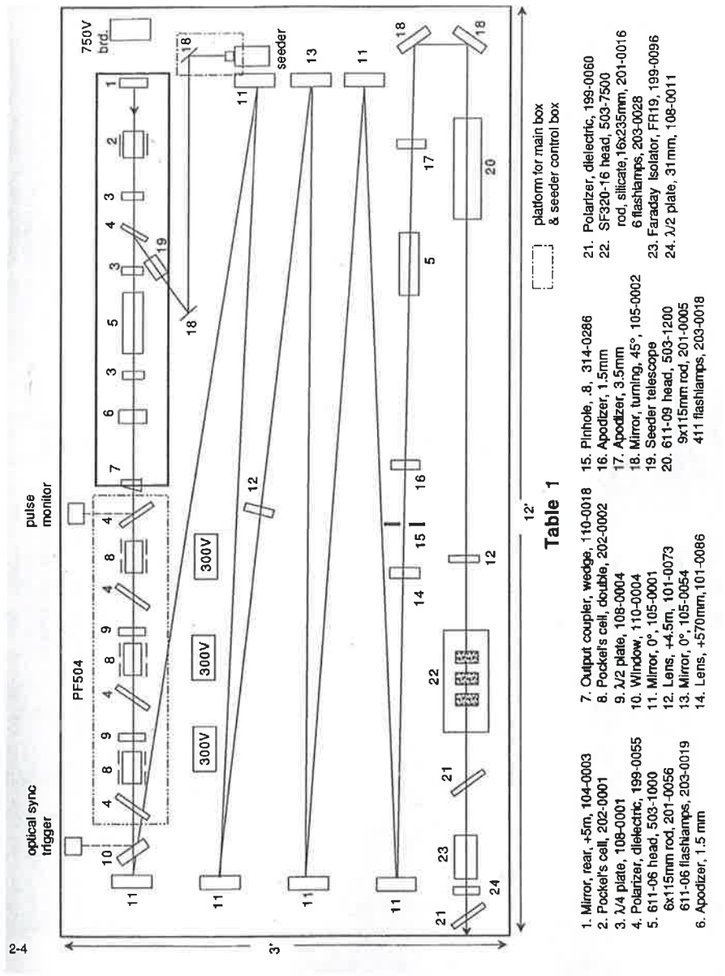

Table 1

1. Mirror, rear, +5m, 104-0003	7. Output coupler, wedge, 110-0018	15. Pinhole, .8, 314-0286
2. Pockel's cell, 202-0001	8. Pockel's cell, double, 202-0002	16. Apodizer, 1.5mm
3. λ/4 plate, 108-0001	9. λ/2 plate, 108-0004	17. Apodizer, 3.5mm
4. Polarizer, dielectric, 199-0055	10. Window, 110-0004	18. Mirror, turning, 45°, 105-0002
5. 611-06 head, 503-1000	11. Mirror, 0°, 105-0001	19. Seeder telescope
6x115mm rod, 201-0056	12. Lens, +4.5m, 101-0073	20. 611-09 head, 503-1200
611-06 flashlamps, 203-0019	13. Mirror, 0°, 105-0054	9x115mm rod, 201-0005
6. Apodizer, 1.5 mm	14. Lens, +570mm, 101-0086	411 flashlamps, 203-0018

Fig. 44a: Nd:glass laser table 1

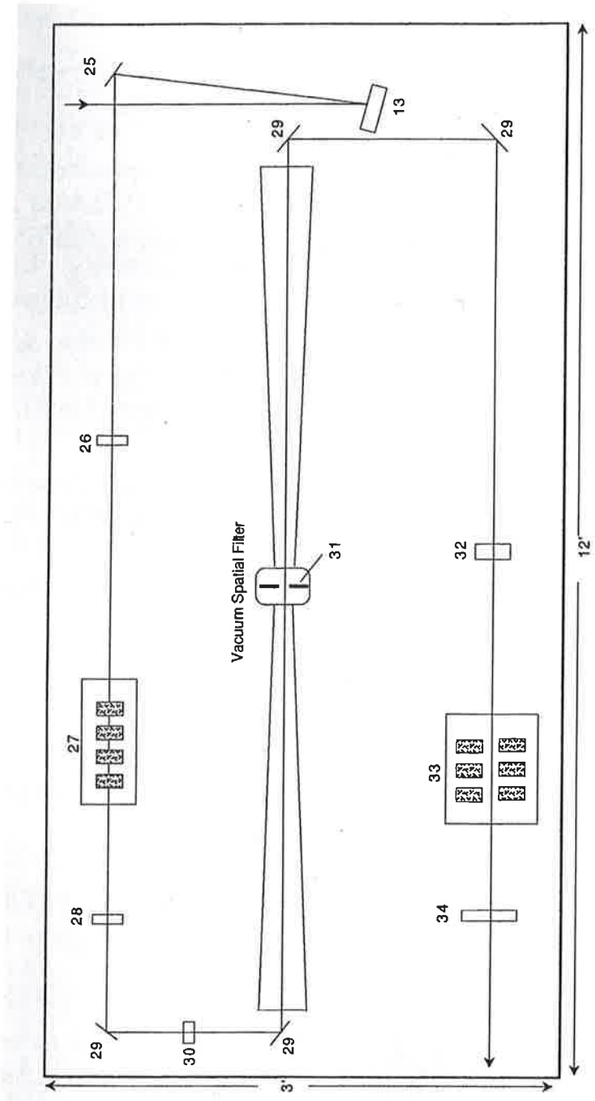

Table 2

25. Mirror, 45°, 2",105-0008	31. Pinhole, 1.7mm	
26. Apodizer, 20mm	32. Apodizer, soft, 40mm	
27. SF320-25 head, 503-8300	33. SF320-45 head, 501-1500	
25x235mm rod, 201-0018	silicate 44x235mm rod, 201-0077	
8 320G flashlamps, 203-0028	12 320G flashlamps (for rods>1")	
28. Lens, +9m, 101-0139	203-0029	
29. Mirror, 45°, 105-0142	34. Lens, +5m (4" optic)	
30. Lens, +2m, 101-0046		

2-5

Fig. 44b: Nd:glass laser table 2

References

[1] Continuum GmbH, *Proposal for a Ti:Sapphire Terawatt Laser*, (April 1993)

[2] K. Yamakawa, P.H. Chiu, A. Magana, and J.D. Kmetec, *Generation of High Peak and Average Power Femtosecond Pulses at a 10 Hz Repetition Rate in a Titanium-Doped Sapphire Laser,* IEEE J. Quantum. Electron. **30**, 2698 (1994)

[3] G. Shvets, N.J. Fisch, A. Pukhov, and J. Meyer-ter-Vehn, *Superradiant Amplification of an Ultra-Short Laser Pulse in a Plasma by a Counter-Propagating Pump,* Phys. Rev. Let. **81**, 4879 (1998)

[4] M. Dreher, *Superradiante Verstärkung ultrakurzer Laserpulse in Plasmen,* Max-Planck-Institut für Quantenoptik, Report **250**, (2000)

[5] M. Born and E. Wolf, *Principles of Optics,* (Pergamon, New York,1979), p. 486

[6] D. Strickland and G. Mourou, *Compression of amplified chirped optical pulses,* Opt. Commun. **56**, 219 (1985)

[7] Coherent, *The Coherent Mira Model 900 Laser,* Operators Manual, (1991)

[8] A. Kasper, *Erzeugung und Charakterisierung ultrakurzer Laserpulse aus Titan:Saphir-Oszillatoren*, Techn. Universität München, PhD thesis, 71 (1997)

[9] A. Leitenstorfer, C. Fürst, and. A. Laubereau, *Widely tunable two-color mode-locked Ti:sapphire laser with pulse jitter of less than 2 fs,* Opt. Let. **20**, 916 (1995)

[10] C. Fürst, A. Leitenstorfer, and A. Laubereau, *Mechanism for Self-Synchronization of Femtosecond Pulses in a Two-Color Ti:Sapphire Laser,* IEEE J. Selected Topics in Quant. Electr., **2**, 473 (1996)

[11] Coherent, *VerdiV-8/V-10 Diode Pumped Lasers,* Operators Manual, (1999)

[12] X. Dong, private communication

[13] M. Pessot, P. Maine, and G. Mourou, *1000 times expansion/compression of optical pulses for chirped pulse amplification*, Opt. Commun. **62**, 419 (1987)

[14] B.E. Lemoff and C.P.J. Barty, *Quintic-phase-limited, spatially uniform expansion and recompression of ultrashort optical pulses*, Opt. Let. **18**, 1651 (1993)

[15] G. Cheriaux, P. Rousseau, F. Salin, J.P. Chambaret, B. Walker, and L.F. Dimauro, *Aberration-free stretcher design for ultrshort-pulse amplification*, Opt. Let. **21**, 414 (1996)

[16] J. Itatani, Y. Nabekawa, K. Kondo, S. Watanabe, *Generation of 13-TW, 26-fs pulses in a Ti:sapphire laser*, Opt. Commun. **134**, 134 (1997)

[17] J.E. Murray and W.H. Lowdermilk, *Nd:YAG regenerative amplifier*, J. Appl. Phys. **51**, 3548 (1980)

[18] Spawr-Industries, *Segmented integrating mirrors*, US-PAT. #4,195,913, (1971)

[19] L.M. Frantz, J.S. Nodvik: J. Appl. Phys. **34**, 2346 (1963)

[20] Spectrogon AB, POB 2076, S-18302 Täby, Sweden

[21] J.C. Diels, J. Fontaine, and W. Rudolph, *Ultrafast diagnostics*, Rev. Phys. Appl.**12**, 1605 (1987)

[22] e.g. see SORL, Space Optics Research Labs, Chelmsford, MA 01824, USA

[23] J.T. Hunt, P.A. Renard, and W.W. Simmons, Appl. Opt. **16**, 779 (1977)

[24] F. Schmid and C.P. Khattak, *Growth of Co:MgF_2 and Ti:Al_2O_3 Crystals for Solid State Laser Applications*, Springer Series in Optical Sciences **47**, 122 (1985)

[25] H.G. Floch, P.F. Belleville, J.J. Priotton et al, *Sol-gel optical coatings for lasers, I, II, and III*, Am. Ceram. Soc. Bull. **74**, No. 10,11,12 (1995)

[26] G. Erbert, I. Bass, R. Hackel, S. Jenkins, K. Kanz, and J. Paisner, *43-W, cw Ti:sapphire* Laser, CLEO 91, OSA Technical Digest Series, 390 (1991)

[27] H. Baumhacker, G. Pretzler, K.J. Witte, M. Hegelich, M. Kaluza, S. Karsch, A. Kudryashov, V. Samarkin, and A. Roukossouev, *Correction of strong phase and amplitude modulations by two deformable mirrors in a multistaged Ti:sapphire laser*, Opt. Let. 27, 1570 (2002)

[28] S. Karsch, private communication

[29] G. Pretzler, A. Kasper, and K.J. Witte, *Angular chirp and tilted light pulses in CPA lasers*, Appl. Phys. B **70**, 1 (2000)

[30] W.J. Smith, *Modern Optical Engineering*, McGraw-Hill, New York, 336 (1990)

[31] B. Platt and R. Shack, Optical Sciences Newsletter **5**, 15 (1971)

[32] G. Artzner, *Microlens arrays for Shack-Hartmann wavefront sensors*, Opt. Eng. **31**, 1311 (1992)

[33] A. Kudryashov, e-mail: kud@laser.ru

[34] M. Nisoli, S. De Silvestri, and O. Svelto, *Generation of high energy 10 fs pulses by a new pulse compression technique*, Appl. Phys. Lett. **68**, 2793 (1996)

[35] T. Wilhelm, J. Piel, and E. Riedle, *Sub-20-fs pulses tunable across the visible from a blue-pumped single-pass noncollinear parametric converter*, Opt. Let. **22**, 1494 (1997)

[36] Yang et al., *Dependence of spectrum on pump-signal angle in BBO-I noncollinear optical-parametric chirped-pulse amplification*, Appl. Phys. B **73**, 219 (2001)

[37] E.T.J. Nibbering, G. Grillon, M.A. Franco, B.S. Prade, and A. Mysyrowicz, *Determination of the inertial contribution to the nonlinear refractive index of air, N_2, and O_2 by use of unfocused high-intensity femtosecond laser pulses*, J. Opt. Soc. Am. B **14**, 650 (1997)